Stretch Regulates Alveologenesis and Homeostasis Via Mesenchymal $G_{\alpha q/11}$-Mediated TGFβ2 Activation

Amanda T Goodwin[1,2,3,*], Alison E John[4], Chitra Joseph[1,2,3], Anthony Habgood[1,2,3], Amanda L Tatler[1,2,3], Katalin Susztak[5], Matthew Palmer[6], Stefan Offermanns[7], Neil C Henderson[8,9], R Gisli Jenkins[4]

[1]Centre for Respiratory Research, Translational Medical Sciences, School of Medicine, University of Nottingham, UK
[2]Nottingham NIHR Biomedical Research Centre, Nottingham, UK
[3]Biodiscovery Institute, University Park, University of Nottingham, Nottingham, UK
[4]National Heart and Lung Institute, Imperial College London, UK
[5]Department of Medicine, Division of Nephrology, University of Pennsylvania Perelman School of Medicine, Philadelphia, USA
[6]Department of Pathology, Division of Nephrology, University of Pennsylvania Perelman School of Medicine, Philadelphia, USA
[7]Max Planck Institute for Heart and Lung Research, Bad Nauheim, Germany
[8]Centre for Inflammation Research, University of Edinburgh, UK
[9]MRC Human Genetics Unit, Institute of Genetics and Molecular Medicine, University of Edinburgh, Edinburgh, UK.

*Correspondence to: Amanda T Goodwin – Amanda.Goodwin@nottingham.ac.uk

Keywords: Alveologenesis; TGFβ; $G_{\alpha q/11}$; GPCR; lung development; cyclical mechanical stretch

Summary statement

Mesenchymal cell $G_{\alpha q/11}$ signalling regulates myofibroblast function and stretch-mediated TGFβ2 signalling, which are important for alveologenesis and organ homeostasis. These mechanisms are relevant to both developmental and adult lung disease.

Abstract

Alveolar development and repair require tight spatiotemporal regulation of numerous signalling pathways that are influenced by chemical and mechanical stimuli. Mesenchymal cells play key roles in numerous developmental processes. Transforming growth factor-β (TGFβ) is essential for alveologenesis and lung repair, and the G protein α subunits $G_{\alpha q}$ and

© 2023. Published by The Company of Biologists Ltd.
This is an Open Access article distributed under the terms of the Creative Commons Attribution License (http://creativecommons.org/licenses/by/4.0), which permits unrestricted use, distribution and reproduction in any medium provided that the original work is properly attributed

Development • Accepted manuscript

$G_{\alpha 11}$ ($G_{\alpha q/11}$) transmit mechanical and chemical signals to activate TGFβ in epithelial cells. To understand the role of mesenchymal $G_{\alpha q/11}$ in lung development, we generated constitutive (*Pdgfrb-Cre*$^{+/-}$;*Gnaq*$^{fl/fl}$;*Gna11*$^{-/-}$) and inducible (*Pdgfrb-Cre/ERT2*$^{+/-}$;*Gnaq*$^{fl/fl}$;*Gna11*$^{-/-}$) mesenchymal $G_{\alpha q/11}$ deleted mice. Mice with constitutive $G_{\alpha q/11}$ gene deletion exhibited abnormal alveolar development, with suppressed myofibroblast differentiation, altered mesenchymal cell synthetic function, and reduced lung TGFβ2 deposition, as well as kidney abnormalities. Tamoxifen-induced mesenchymal $G_{\alpha q/11}$ gene deletion in adult mice resulted in emphysema associated with reduced TGFβ2 and elastin deposition. Cyclical mechanical stretch-induced TGFβ activation required $G_{\alpha q/11}$ signalling and serine protease activity, but was independent of integrins, suggesting an isoform-specific role for TGFβ2 in this model. These data highlight a previously undescribed mechanism of cyclical stretch-induced $G_{\alpha q/11}$-dependent TGFβ2 signalling in mesenchymal cells, which is imperative for normal alveologenesis and maintenance of lung homeostasis.

Introduction

Normal alveologenesis requires tight spatiotemporal control of numerous molecular signalling pathways, and coordinated crosstalk between multiple cell types. Any perturbation to these complex processes can disrupt alveolar formation, resulting in structural and functional abnormalities to the gas exchange regions of the lungs. Such abnormalities contribute to perinatal death and lifelong lung function disturbances in survivors (Lovering et al., 2014). The alveolar stage is the final phase of lung development, during which primitive pulmonary sacculi are divided by newly formed secondary septa to form mature alveoli. Alveolarisation occurs between 36 weeks gestation to around 6 years of age in humans (Donahoe et al., 2016), and postnatal days 3-30 (P3-P30) in mice (Beauchemin et al., 2016; Li et al., 2015; Pozarska et al., 2017), therefore postnatal exposures and stimuli are key influences in alveolar development. Many pathways that drive normal lung development are also instrumental in adult lung repair (Chanda et al., 2019), therefore understanding normal lung development could have implications for numerous pulmonary diseases.

Mesenchymal cells include various cell types that are integral to normal developmental processes, and pericytes are perivascular cells widely considered to be mesenchymal precursors in the lung (Barron et al., 2016; Kato et al., 2018; Ricard et al., 2014). Pericytes express platelet-derived growth factor receptor-β (PDGFRβ), PDGFRα, and neural/ glial antigen 2 (NG2), among other markers. However the most specific marker for pericytes is PDGFRβ (Riccetti et al., 2020), and PDGFRβ co-expression with other pericyte markers correlates with the expected location of pericytes in the lung (Henderson et al., 2013). Pericytes migrate and differentiate into parenchymal myofibroblasts in the lung, as well as

Development • Accepted manuscript

other mesenchymal cell types. Myofibroblast-driven deposition of extracellular matrix (ECM) proteins, such as collagen and elastin, provide the scaffolds for secondary septation during lung development and lung repair (Mecham, 2018; Mizikova and Morty, 2015). Therefore pericytes, and the mesenchymal cells that derive from them, are instrumental in alveologenesis and lung homeostasis.

The pleiotropic growth factor transforming growth factor-β (TGFβ) regulates numerous developmental and repair processes, including the proliferation, migration, and differentiation of pericytes and other mesenchymal cells (Bartram and Speer, 2004), as well as the generation of extracellular matrix (ECM). TGFβ signalling is tightly regulated in vivo by the production of TGFβ in latent form, and the three mammalian TGFβ isoforms, TGFβ1, TGFβ2, and TGFβ3, must be activated to exert their biological effects. While TGFβ signalling is essential for multiple processes in alveolar development and repair (Bartram and Speer, 2004), the mechanisms that control TGFβ activation in alveologenesis are unclear.

Latent TGFβ is activated when a conformational change to the large latent complex alters the relationship between TGFβ and the latency associated peptide, allowing TGFβ to interact with its receptor. The G-proteins $G_{\alpha q}$ and $G_{\alpha 11}$ ($G_{\alpha q/11}$) mediate TGFβ activation in response to G-protein-coupled receptor (GPCR)-ligand binding as well as mechanical stretch in epithelial cells (John et al., 2016; Xu et al., 2009). GPCR signalling has also been implicated in normal alveologenesis (Funke et al., 2016). Cyclical mechanical stretch (CMS) has been shown to induce TGFβ activation in lung slices via a Rho-associated kinase (ROCK)- and αv integrin-dependent process (Froese et al., 2016), although the contribution to this by individual cell types is unknown. While stretch secondary to foetal breathing movements in utero is essential for early lung development (Donahoe et al., 2016), the role of breathing-related CMS specifically in mesenchymal cells in alveolar development and the maintenance of adult alveoli has not been investigated.

We hypothesised that $G_{\alpha q/11}$ would mediate CMS-induced TGFβ activation via ROCK and integrin signalling in mesenchymal cells, and that this would be important in alveologenesis and lung homeostasis. Here we show, using mesenchymal $G_{\alpha q/11}$ knockout mouse models and an in vitro CMS system, that mesenchymal $G_{\alpha q/11}$ is essential for normal alveologenesis and maintenance of adult alveoli via CMS-induced TGFβ signalling, but that this occurs in a ROCK- and integrin-independent manner via a pathway likely to involve the TGFβ2 isoform.

Development • Accepted manuscript

Results

Pdgfrb-Cre$^{+/-}$*;Gnaq*$^{fl/fl}$*;Gna11*$^{-/-}$ mice are growth restricted and are not viable beyond P24

To understand whether mesenchymal $G_{\alpha q/11}$ deletion resulted in detrimental effects in vivo, gross phenotypes and genotype frequencies of offspring from the *Pdgfrb-Cre*$^{+/-}$ *x* *Gnaq*$^{fl/fl}$*;Gna11*$^{-/-}$ crosses were analysed. Fewer mesenchymal $G_{\alpha q/11}$ knockout (*Pdgfrb-Cre*$^{+/-}$*;Gnaq*$^{fl/fl}$*;Gna11*$^{-/-}$) pups reached genotyping age (postnatal day 14, P14) than was expected (6.6% observed compared with 12.5% expected, Chi squared value = 22.03, p<0.005, **Fig. 1A**). Conversely, mice with at least one functional mesenchymal *Gnaq* or *Gna11* allele reached genotyping age at rates closer to the expected Mendelian frequencies (**Fig. 1A**). Furthermore, *Pdgfrb-Cre*$^{+/-}$*;Gnaq*$^{fl/fl}$*;Gna11*$^{-/-}$ pups were notably smaller than littermates with at least one intact mesenchymal *Gnaq* or *Gna11* allele. *Pdgfrb-Cre*$^{+/-}$*;Gnaq*$^{fl/fl}$*;Gna11*$^{-/-}$ animals had a mean weight 1.9-3.2g lower than all other genotypes (5.4g vs 7.3-8.4g, p<0.03 **Fig. 1B**). *Pdgfrb-Cre*$^{+/-}$*;Gnaq*$^{fl/fl}$*;Gna11*$^{-/-}$ pups were also smaller in physical size compared with control animals (**Fig. 1C**). There was no sex-related difference in weight across genotypes (**Fig. 1D**). These findings indicate that mesenchymal $G_{\alpha q/11}$ deletion causes a detrimental developmental phenotype, leading to death in utero or in early life.

The first two *Pdgfrb-Cre*$^{+/-}$*;Gnaq*$^{fl/fl}$*;Gna11*$^{-/-}$ mice from this breeding programme were humanely killed due to poor physical condition at P21 and P24. Therefore, all further analyses were performed in P14 mice, before evidence of ill health was observed. *Gnaq*$^{fl/fl}$*;Gna11*$^{-/-}$ mice develop normally and do not express a phenotype (John et al., 2016), therefore *Pdgfrb-Cre*$^{-/-}$*;Gnaq*$^{fl/fl}$*;Gna11*$^{-/-}$ littermates were used as controls for all analyses to ensure that control mice had an identical genotype to the mesenchymal $G_{\alpha q/11}$ knockout mice other than Cre expression, and to facilitate the use of age-matched littermate controls. From here, mice with the *Pdgfrb-Cre*$^{-/-}$*;Gnaq*$^{fl/fl}$*;Gna11*$^{-/-}$ genotype will be referred to as *Gna11*$^{-/-}$ controls.

Pdgfrb-Cre$^{+/-}$*;Gnaq*$^{fl/fl}$*;Gna11*$^{-/-}$ mice have impaired alveologenesis.

To understand the role of mesenchymal $G_{\alpha q/11}$ signalling in lung development, the lungs of *Pdgfrb-Cre*$^{+/-}$*;Gnaq*$^{fl/fl}$*;Gna11*$^{-/-}$ mice and *Gna11*$^{-/-}$ controls were examined histologically. *Pdgfrb-Cre*$^{+/-}$*;Gnaq*$^{fl/fl}$*;Gna11*$^{-/-}$ mouse lungs exhibited clear abnormalities consistent with impaired alveolar development at P14 (**Fig. 2A**). *Pdgfrb-Cre*$^{+/-}$*;Gnaq*$^{fl/fl}$*;Gna11*$^{-/-}$ lungs contained enlarged airspaces with a mean linear intercept distance of 63.47µm compared with 36.43µm in *Gna11*$^{-/-}$ mice (p=0.03, **Fig. 2B**), thickened alveolar walls of 12.2µm

Development • Accepted manuscript

compared with 7.0µm in *Gna11*$^{-/-}$ controls (p=0.03, **Fig. 2C**), and fewer secondary crests (53.7 vs 107.2 per field, p=0.03, **Fig. 2D**) relative to *Gna11*$^{-/-}$ littermate controls. Mice with at least one expressed *Gnaq* or *Gna11* allele (i.e. any genotype other than *Pdgfrb-Cre*$^{+/-}$*;Gnaq*$^{fl/fl}$*;Gna11*$^{-/-}$) had normal lung histological appearances and similar morphometric measurements that differed from those of *Pdgfrb-Cre*$^{+/-}$*;Gnaq*$^{fl/fl}$*;Gna11*$^{-/-}$ mice (**Fig. S1**), indicating that a complete absence of *Gnaq* and *Gna11* in mesenchymal cells is required for the abnormal lung phenotype to be observed. These data also demonstrate that Cre expression or presence of the floxed Gnaq alleles alone do not influence the lung phenotype observed in *Pdgfrb-Cre*$^{+/-}$*;Gnaq*$^{fl/fl}$*;Gna11*$^{-/-}$ mice.

In addition to these structural abnormalities, *Pdgfrb-Cre*$^{+/-}$*;Gnaq*$^{fl/fl}$*;Gna11*$^{-/-}$ lungs expressed lower levels of the proliferative marker Ki67 than *Gna11*$^{-/-}$ controls, with 16% of cell nuclei staining positively for Ki67 in *Pdgfrb-Cre*$^{+/-}$*;Gnaq*$^{fl/fl}$*;Gna11*$^{-/-}$ lungs compared with 26% in *Gna11*$^{-/-}$ controls (p=0.03, **Fig. 2A, 2E**). Furthermore, *Pdgfrb-Cre*$^{+/-}$*;Gnaq*$^{fl/fl}$*;Gna11*$^{-/-}$ lungs contained a lower proportion of cells staining positively for the type II epithelial cell marker pro-surfactant protein C (pro-SPC) than *Gna11*$^{-/-}$ control lungs, at 8.9% and 12.8% of all cells, respectively (p=0.03, **Fig. 2A, 2F**).

Finally, *Pdgfrb-Cre*$^{+/-}$*;Gnaq*$^{fl/fl}$*;Gna11*$^{-/-}$ lungs were heavier relative to total body weight compared with lungs from *Gna11*$^{-/-}$ mice (16.5 vs 14.3mg/g total body weight, p<0.01, **Fig. 2G**), which could be due to elevated lung density or interstitial oedema in these animals. This trend of increased lung weight in *Pdgfrb-Cre*$^{+/-}$*;Gnaq*$^{fl/fl}$*;Gna11*$^{-/-}$ mice was also observed when compared to all other genotypes possible from this breeding strategy (**Fig. S1**). Overall, these structural, proliferative, and cellular differentiation abnormalities indicate a disturbance to alveologenesis in *Pdgfrb-Cre*$^{+/-}$*;Gnaq*$^{fl/fl}$*;Gna11*$^{-/-}$ mice.

Myofibroblast differentiation and function is defective in *Pdgfrb-Cre*$^{+/-}$*;Gnaq*$^{fl/fl}$*;Gna11*$^{-/-}$ mouse lungs

Myofibroblasts are essential for normal alveolar development, therefore studies were undertaken to assess myofibroblast differentiation and function in *Pdgfrb-Cre*$^{+/-}$*;Gnaq*$^{fl/fl}$*;Gna11*$^{-/-}$ lungs.

Immunohistochemical staining for the myofibroblast marker α-smooth muscle actin (αSMA) demonstrated fewer myofibroblasts in the lungs of P14 *Pdgfrb-Cre*$^{+/-}$*;Gnaq*$^{fl/fl}$*;Gna11*$^{-/-}$ mice compared with *Gna11*$^{-/-}$ littermate controls (**Fig. 3A**). While overall αSMA staining was decreased in *Pdgfrb-Cre*$^{+/-}$*;Gnaq*$^{fl/fl}$*;Gna11*$^{-/-}$ lungs, there was no significant reduction in the proportion of αSMA-positive secondary crests compared with *Gna11*$^{-/-}$ lungs (0.69 vs 0.84 in controls, p =0.2, **Fig. 3B**).

Development • Accepted manuscript

To investigate whether $G_{\alpha q/11}$ knockout influences myofibroblast differentiation, murine embryonic fibroblasts (MEFs) that were wild-type (WT), $G_{\alpha q/11}$ deficient (*Gnaq*$^{-/-}$;*Gna11*$^{-/-}$) or $G_{\alpha 12/13}$ deficient (*Gna12*$^{-/-}$;*Gna13*$^{-/-}$) were assessed for αSMA protein and *Acta2* mRNA expression. MEFs with a stable $G_{\alpha q/11}$ knockout had lower *Acta2* mRNA (**Fig. 3C**) and αSMA protein expression than WT MEFs, whereas MEFs lacking $G_{\alpha 12/13}$, another G_{α} subunit family, did not have significantly different αSMA expression compared with WT cells (**Fig. 3D, 3E**). This implies a key role for $G_{\alpha q/11}$ signalling in the differentiation of myofibroblasts from mesenchymal precursor cells.

Pdgfrb-Cre$^{+/-}$;*Gnaq*$^{fl/fl}$;*Gna11*$^{-/-}$ lungs also showed evidence of defective myofibroblast synthetic function. *Pdgfrb-Cre*$^{+/-}$;*Gnaq*$^{fl/fl}$;*Gna11*$^{-/-}$ lungs contained fewer elastin foci (7.4 vs 24.9 foci per field, p=0.03, **Fig. 3A & 3F**) and fewer elastin-positive secondary crests (57.5% vs 84.8%, p=0.03, **Fig. 3G**) than *Gna11*$^{-/-}$ mouse lungs. Furthermore, picrosirius red staining revealed that P14 *Pdgfrb-Cre*$^{+/-}$;*Gnaq*$^{fl/fl}$;*Gna11*$^{-/-}$ mouse lungs contained less collagen than the lungs of *Gna11*$^{-/-}$ controls (**Fig. 3A**). These data were supported by lower *Eln*, *Col1a1* and *Col3a1* mRNA expression in *Gnaq*$^{-/-}$;*Gna11*$^{-/-}$ MEFs than WT MEFs (**Fig. 3H-J**). These findings imply a failure of myofibroblast differentiation in the lungs of mice lacking mesenchymal $G_{\alpha q/11}$ associated with a reduction in myofibroblast function, leading to a reduction in subepithelial matrix deposition.

Pdgfrb-Cre$^{+/-}$;*Gnaq*$^{fl/fl}$;*Gna11*$^{-/-}$ mice have abnormal peripheral pulmonary vessels

Pericytes are *Pdgfrb*-expressing cells that originate in the perivascular region (Henderson et al., 2013), and vasculogenesis is an important driver of normal lung development. Therefore, we examined the pulmonary vasculature histologically to assess for abnormalities caused by mesenchymal $G_{\alpha q/11}$ deletion. P14 *Pdgfrb-Cre*$^{+/-}$;*Gnaq*$^{fl/fl}$;*Gna11*$^{-/-}$ lungs contained markedly abnormal peripheral pulmonary vessels (**Fig. 4A-G**), with significantly thicker walls (mean ratio of vessel wall thickness: vessel diameter 0.45 vs 0.33µm, p=0.03, **Fig. 4H**) and reduced vessel lumen diameter (mean ratio of internal vessel diameter: whole vessel diameter of 0.54 compared with 0.67, p=0.03, **Fig. 4I**) than the peripheral pulmonary vessels of *Gna11*$^{-/-}$ controls. These vessels consisted of a thin CD31 positive endothelial layer (**Fig. 4B**) surrounded by a thickened αSMA positive vascular smooth muscle layer (**Fig. 4C**) without increased proliferation (Ki67 positive; **Fig. 4D**), indicating that the smooth muscle layer was hypertrophic rather than hyperplastic. These abnormal vessels did not contain significant collagen or elastin layers (**Fig. 4E-G)**. CD31 staining of the alveoli of *Pdgfrb-Cre*$^{+/-}$;*Gnaq*$^{fl/fl}$;*Gna11*$^{-/-}$ lungs had a similar appearance to those seen in *Gna11*$^{-/-}$ lungs at high

Development • Accepted manuscript

magnification (**Fig. 4J**). This argues against there being gross abnormality of the small alveolar vessels, however this cannot be completely ruled out.

Given that there were some similarities in appearance of the abnormal peripheral pulmonary vasculature in *Pdgfrb-Cre*$^{+/-}$*;Gnaq*$^{fl/fl}$*;Gna11*$^{-/-}$ lungs to those seen in pulmonary arterial hypertension, we assessed the hearts from these animals for evidence of right ventricular hypertrophy. We found no difference in right: left ventricular wall ratio in *Pdgfrb-Cre*$^{+/-}$*;Gnaq*$^{fl/fl}$*;Gna11*$^{-/-}$ mice relative to controls (**Fig. 4K-L**). These data suggest a primary *Pdgfrb*$^{+}$ cell-driven defect, rather than secondary pulmonary hypertension due to impaired alveologenesis.

Pdgfrb-Cre$^{+/-}$*;Gnaq*$^{fl/fl}$*;Gna11*$^{-/-}$ mice have kidney abnormalities

As *Pdgfrb* expression is not exclusive to lung mesenchymal cells, the kidneys, hearts, livers, and bowel of *Pdgfrb-Cre*$^{+/-}$*;Gnaq*$^{fl/fl}$*;Gna11*$^{-/-}$ mice were assessed for extrapulmonary abnormalities.

We observed an expansion and prominence of medullary mesenchymal cells in *Pdgfrb-Cre*$^{+/-}$*;Gnaq*$^{fl/fl}$*;Gna11*$^{-/-}$ kidneys demonstrated by αSMA and PDGFRβ staining (**Fig. 5A**), with associated thinning of the cortex (median cortex: medulla ratio 0.31 in *Pdgfrb-Cre*$^{+/-}$*;Gnaq*$^{fl/fl}$*;Gna11*$^{-/-}$ kidneys and 0.43 in *Gna11*$^{-/-}$ controls, p<0.03, **Fig. 5B, C**). The relative kidney to total body weight values of *Pdgfrb-Cre*$^{+/-}$*;Gnaq*$^{fl/fl}$*;Gna11*$^{-/-}$ mouse kidneys were not different to *Gna11*$^{-/-}$ controls (median kidney: total body weight ratio 7.3 in *Pdgfrb-Cre*$^{+/-}$*;Gnaq*$^{fl/fl}$*;Gna11*$^{-/-}$ mice and 6.5 in *Gna11*$^{-/-}$ controls, p=0.55; **Fig. 5D**). These data suggest that mesenchymal $G_{\alpha q/11}$ is important in normal kidney development.

Pdgfrb-Cre$^{+/-}$*;Gnaq*$^{fl/fl}$*;Gna11*$^{-/-}$ mice had normal heart, liver and bowel histology (**Fig. S2**), suggesting that mesenchymal $G_{\alpha q/11}$ signalling is not required for normal heart, liver, or bowel development or homeostasis from conception to P14 in mice.

Mice with mesenchymal $G_{\alpha q/11}$ knockout induced in adulthood have emphysema with altered ECM, but no extrapulmonary abnormalities

To assess whether the abnormalities seen in *Pdgfrb-Cre*$^{+/-}$*;Gnaq*$^{fl/fl}$*;Gna11*$^{-/-}$ mice were related solely to disturbed organ developmental processes or could also affect mature lungs, a tamoxifen-inducible mesenchymal $G_{\alpha q/11}$ knockout model (*Pdgfrb-Cre/ERT2*$^{+/-}$*;Gnaq*$^{fl/fl}$*;Gna11*$^{-/-}$) was conducted in adult mice (**Fig. 6A)**.

Tamoxifen-naïve *Pdgfrb-Cre/ERT2*$^{+/-}$*;Gnaq*$^{fl/fl}$*;Gna11*$^{-/-}$ mice were born at the expected frequency. According to the supplier, it is expected that 20% of offspring from breeding of the Cre-expressing hemizygous mice with wild type mice will express the *Pdgfrb-Cre/ERT2*

Development • Accepted manuscript

transgene (Jackson Laboratory), rather than the 50% Cre-expression rate observed in the germline *Pdgfrb-Cre*$^{+/-}$ mouse colony. The frequency of *Pdgfrb-Cre/ERT2*$^{+/-}$;*Gnaq*$^{fl/fl}$;*Gna11*$^{-/-}$ mice reaching genotyping age was 6.4%, compared with the expected 5% (total number of mice born 109; **Fig. 6B)**. This indicates that having the *Pdgfrb-Cre/ERT2*$^{+/-}$;*Gnaq*$^{fl/fl}$;*Gna11*$^{-/-}$ genotype, without administration of tamoxifen, does not cause any gross developmental defects.

When a three week course of tamoxifen was administered to P49 *Pdgfrb-Cre/ERT2*$^{+/-}$;*Gnaq*$^{fl/fl}$;*Gna11*$^{-/-}$ mice (n=4, 1 female 3 male), no detrimental effect to health status was observed compared with littermate controls. Furthermore, *Pdgfrb-Cre/ERT2*$^{+/-}$;*Gnaq*$^{fl/fl}$;*Gna11*$^{-/-}$ mice gained weight at the same rate as littermate controls with the other genotypes during the tamoxifen protocol (median weight on day 21 of tamoxifen 104.3% of baseline in *Pdgfrb-Cre/ERT2*$^{+/-}$;*Gnaq*$^{fl/fl}$;*Gna11*$^{-/-}$ mice compared to 106.2% of baseline in other genotypes, p=0.71; **Fig. 6C**). A small reduction in weight was observed early in the tamoxifen protocol that was independent of genotype and was in keeping with a change in diet (Kiermayer et al., 2007). These data suggest that short-term mesenchymal $G_{\alpha q/11}$ knockout does not cause gross physiological disturbances *in vivo*.

On histological analysis, the lungs of *Pdgfrb-Cre/ERT2*$^{+/-}$;*Gnaq*$^{fl/fl}$;*Gna11*$^{-/-}$ mice treated with tamoxifen demonstrated increased airspace size compared with *Gna11*$^{-/-}$ controls (mean linear intercept distance 52.5µm in *Pdgfrb-Cre/ERT2*$^{+/-}$;*Gnaq*$^{fl/fl}$;*Gna11*$^{-/-}$ mice compared with 39.3µm in *Gna11*$^{-/-}$ controls, p=0.03, **Fig. 6D, 6E**), suggestive of emphysema. *Pdgfrb-Cre/ERT2*$^{+/-}$;*Gnaq*$^{fl/fl}$;*Gna11*$^{-/-}$ lungs contained fewer elastin foci than *Gna11*$^{-/-}$ controls after three weeks of tamoxifen (median number of elastin foci per high powered field 13.0 in *Pdgfrb-Cre/ERT2*$^{+/-}$;*Gnaq*$^{fl/fl}$;*Gna11*$^{-/-}$ mice compared with 26.9 in *Gna11*$^{-/-}$ controls, p=0.03, **Fig. 6D, 6F**), similar to the constitutive knockout. In contrast, *Pdgfrb-Cre/ERT2*$^{+/-}$;*Gnaq*$^{fl/fl}$;*Gna11*$^{-/-}$ lungs did not exhibit altered collagen deposition or evidence of fewer myofibroblasts (αSMA) when compared with *Gna11*$^{-/-}$ controls (**Fig. 6D**). Three of the four *Pdgfrb-Cre/ERT2*$^{+/-}$;*Gnaq*$^{fl/fl}$;*Gna11*$^{-/-}$ mice also exhibited abnormal pulmonary mononuclear cellular aggregates which predominated at the pleural surfaces (**Fig. 6G**), and were not observed in littermate control mice. Despite these abnormalities, *Pdgfrb-Cre/ERT2*$^{+/-}$;*Gnaq*$^{fl/fl}$;*Gna11*$^{-/-}$ mice did not exhibit signs of respiratory distress.

In contrast with *Pdgfrb-Cre*$^{+/-}$;*Gnaq*$^{fl/fl}$;*Gna11*$^{-/-}$ mice, *Pdgfrb-Cre/ERT2*$^{+/-}$;*Gnaq*$^{fl/fl}$;*Gna11*$^{-/-}$ mice administered tamoxifen did not exhibit any renal abnormalities on histology (**Fig. S3**). This implies that mesenchymal $G_{\alpha q/11}$ is needed for normal kidney development, but not maintenance of the normal kidney.

Development • Accepted manuscript

Cyclical mechanical stretch-induced TGFβ activation in fibroblasts requires $G_{\alpha q/11}$, but not ROCK or αv or β1 integrins

Given the crucial roles of TGFβ in alveolar development, lung repair, and mesenchymal cell migration and differentiation, we investigated the role of mesenchymal $G_{\alpha q/11}$ in a cyclical stretch model of TGFβ activation. Mesenchymal cells with and without intact $G_{\alpha q/11}$ signalling were subjected to breathing-related CMS and TGFβ signalling was assessed. CMS-induced TGFβ signalling, as assessed by Smad2 phosphorylation, was significantly reduced in *Gnaq*$^{-/-}$;*Gna11*$^{-/-}$ MEFs compared with WT MEFs (**Fig. 7A-B)**. This finding was specific to the $G_{\alpha q/11}$ family of G proteins, as there was no effect of $G_{\alpha 12/13}$ knockdown on stretch-induced TGFβ signalling in MEFs (**Fig. 7A**).

To validate the role of $G_{\alpha q/11}$ in stretch-induced TGFβ signalling in mesenchymal cells across species, human lung fibroblasts (HLFs) with and without siRNA-induced *GNAQ* and *GNA11* knockdown were subjected to breathing-related CMS. *GNAQ* and *GNA11* siRNA led to substantial reductions in both $G_{\alpha q}$ and $G_{\alpha 11}$ protein expression in HLFs, and significantly reduced CMS-induced TGFβ signalling compared with scrambled control (Scr) siRNA as measured by phosphorylation of Smad2 (**Fig. 7C-D**). These data indicate that $G_{\alpha q/11}$ is a key component of CMS-induced TGFβ signalling in both murine and human fibroblasts.

Previous studies have reported that $G_{\alpha q/11}$ induces TGFβ activation via the Rho-ROCK cascade and αv integrins in epithelial cells (Froese et al., 2016; Xu et al., 2009). As αvβ1, αvβ3, and αvβ5 integrins are expressed by myofibroblasts and are involved in TGFβ activation (Pakshir et al., 2020), we utilised chemical inhibition of these integrins and ROCK in our CMS model. When human fibroblasts were subject to breathing-related CMS in the presence of a ROCK1/2 inhibitor (Y27632), a pan αv integrin inhibitor (CWHM-12) or a β1 integrin-specific inhibitor (NOTT199SS), CMS-induced TGFβ signalling was not reduced (**Fig. S4**). These data imply a novel pathway for CMS-induced TGFβ signalling in mesenchymal cells which requires $G_{\alpha q/11}$, but is independent of ROCK and integrin signalling.

$G_{\alpha q/11}$ induces TGFβ2 production, which is then available for CMS-induced serine protease-mediated activation

Proteases can activate latent TGFβ independently of integrins, therefore we assessed the effect of protease inhibitors in our CMS-induced TGFβ signalling system. A pan serine protease inhibitor 4-(2-aminoethyl)benzenesulfonyl fluoride (AEBSF), decreased CMS-induced Smad2 phosphorylation in HLFs (**Fig. 8A-B**), whereas the matrix metalloproteinase (MMP) inhibitor GM-6001 had no effect on CMS-induced TGFβ signalling even at high

Development • Accepted manuscript

concentrations (**Fig. 8C-D**). These findings indicate that serine proteases mediate CMS-induced TGFβ signalling in mesenchymal cells.

As TGFβ2 is the only TGFβ isoform that is not activated by integrins (Jenkins, 2008), we hypothesised that breathing-related CMS would predominantly activate the TGFβ2 isoform in mesenchymal cells. While CMS did not influence TGFβ2 protein expression in HLFs, HLFs with siRNA-induced *GNAQ* and *GNA11* knockdown expressed less TGFβ2 than HLFs with intact $G_{\alpha q/11}$ signalling (**Fig. 8E-F**), suggesting that $G_{\alpha q/11}$ plays a role in TGFβ2 production. Conversely, TGFβ1 protein expression was not affected by *GNAQ* and *GNA11* knockdown in HLFs (**Fig. 8G**), suggesting an isoform-specific effect.

To evaluate the role of this CMS-induced TGFβ2 signalling pathway in alveologenesis, we assessed TGFβ2 expression in the lungs of mice from our mouse models. *Pdgfrb-Cre*$^{+/-}$*;Gnaq*$^{fl/fl}$*;Gna11*$^{-/-}$ lungs had a significantly lower TGFβ2 content than *Gna11*$^{-/-}$ control lungs (median immunostaining score 0.8 in *Pdgfrb-Cre*$^{+/-}$*;Gnaq*$^{fl/fl}$*;Gna11*$^{-/-}$ lungs, compared with 2.7 in *Gna11*$^{-/-}$ controls, p<0.03, **Fig. 8H, 8I**). Similarly, *Pdgfrb-Cre/ERT2*$^{+/-}$*;Gnaq*$^{fl/fl}$*;Gna11*$^{-/-}$ mouse lungs also had reduced TGFβ2 deposition compared with *Gna11*$^{-/-}$ controls after 3 weeks of tamoxifen (median immunostaining score 0.8 in *Pdgfrb-Cre/ERT2*$^{+/-}$*;Gnaq*$^{fl/fl}$*;Gna11*$^{-/-}$ lungs compared with 2.2 in *Gna11*$^{-/-}$ controls, p<0.03, **Fig. 8H, 8J**). These data demonstrate that lungs lacking mesenchymal $G_{\alpha q/11}$ have less TGFβ2 available for breathing-related CMS-induced activation, and this may be important in alveologenesis and the maintenance of normal lung structure in vivo.

$G_{\alpha q/11}$ influences expression of PDGF signalling components

Platelet-derived growth factor (PDGF) signalling is known to be important in alveolar development, and this pathway interacts with TGFβ signalling in normal development and disease (Gouveia et al., 2017; Gouveia et al., 2018). We therefore investigated how $G_{\alpha q/11}$ signalling influences the expression of PDGF signalling components in fibroblasts.

Gnaq$^{-/-}$*;Gna11*$^{-/-}$ MEFs expressed significantly lower levels of *Pdgfb* and *Pdgfd* mRNA compared with wild-type cells (p=0.03, **Fig. 9B, 9D**). There was not a statistically significant difference in the expression of *Pdgfa*, *Pdgfc*, *Pdgfra*, or *Pdgfrb* mRNA expression between *Gnaq*$^{-/-}$*;Gna11*$^{-/-}$ and wild-type MEFs (**Fig. 9A,C,E,F**), although there was a trend to reduced *Pdgfa* expression in *Gnaq*$^{-/-}$*;Gna11*$^{-/-}$ MEFs (p=0.06, **Fig. 9A**). These data imply that mesenchymal $G_{\alpha q/11}$ deletion influences the expression of PDGF signalling components, and thus may regulate PDGF signalling.

Development • Accepted manuscript

Discussion

In this study, we used mice with a targeted deletion of $G_{\alpha q/11}$ in *Pdgfrb*-expressing cells to demonstrate that mesenchymal $G_{\alpha q/11}$ is essential for the development and maintenance of normal alveoli. Loss of $G_{\alpha q/11}$-mediated signalling in mesenchymal cells caused failure of the myofibroblast differentiation and ECM synthetic function required for alveolar development and the maintenance of the adult lung, and reduced mesenchymal cell TGFβ2 production is a key factor in these processes. In the absence of mesenchymal $G_{\alpha q/11,}$ TGFβ2 is unavailable for activation by CMS-induced serine proteases thereby diminishing downstream TGFβ signalling in both developing and adult lungs. These findings establish a previously undescribed role for breathing-related CMS in TGFβ2 generation, and suggest a role for TGFβ2 in alveolar development and lung homeostasis.

The role of $G_{\alpha q/11}$ in alveolar development has not previously been investigated, primarily because germline $G_{\alpha q/11}$ deletion is embryonically lethal (Offermanns et al., 1998) and murine alveolarisation occurs entirely postnatally (Beauchemin et al., 2016). Cell type-specific *Gnaq* and *Gna11* deletion in neural, cardiovascular, and haematological tissues have various manifestations ranging from no phenotype to profound cardiac abnormalities associated with perinatal death (Hoyer et al., 2010; Sassmann et al., 2010; Wettschureck et al., 2007; Wettschureck et al., 2004; Wettschureck et al., 2005; Wettschureck et al., 2001; Wettschureck et al., 2006). However, alveolar abnormalities have not been described in germline or conditional $G_{\alpha q/11}$ knockout mice, suggesting a unique role for mesenchymal $G_{\alpha q/11}$ in alveolar development and maintenance.

We propose that the key mechanisms underlying the abnormal alveologenesis and emphysema in mice with mesenchymal $G_{\alpha q/11}$ deletion present from conception or induced in adulthood, respectively, are failure of myofibroblast differentiation and synthetic function. Both *Pdgfrb-Cre*$^{+/-}$;*Gnaq*$^{fl/fl}$;*Gna11*$^{-/-}$ and *Pdgfrb-Cre/ERT2*$^{+/-}$;*Gnaq*$^{fl/fl}$;*Gna11*$^{-/-}$ mice had lower lung elastin deposition than controls. *Pdgfrb-Cre*$^{+/-}$;*Gnaq*$^{fl/fl}$;*Gna11*$^{-/-}$ lungs also contained fewer myofibroblasts and less collagen compared with controls, and mesenchymal cells lacking $G_{\alpha q/11}$ express less *Col1a1*, *Col3a1*, and *Eln* mRNA than cells with intact $G_{\alpha q/11}$. As myofibroblasts induce secondary septation by depositing ECM proteins, particularly elastin, at the tips of developing secondary septa (Dabovic et al., 2015), and loss of elastin is a key feature of emphysema (Ito et al., 2019; Suki et al., 2012), these data suggest that mesenchymal $G_{\alpha q/11}$-induced myofibroblast differentiation and function are required for alveolar development and homeostasis. In addition, as elastin is a key factor governing lung compliance (Dolhnikoff et al., 1999; Hilgendorff et al., 2012), and mechanical forces themselves may alter availability of elastin binding sites (Jesudason et al., 2010; Suki et al., 2012), elastin may influence the response to stretch-related forces. Therefore, the impact of

Development • Accepted manuscript

mesenchymal $G_{\alpha q/11}$ deletion on elastin deposition and distribution may influence the response to and generation of mechanical forces within the lungs.

Secondary crest myofibroblasts (SCMFs) are known to derive from PDGFRα-expressing precursors (Boström et al., 1996; Li et al., 2018; Lindahl et al., 1997; McGowan et al., 2008), however the role of PDGRFβ$^+$ precursors in the development of SCMFs has not been described. While this study cannot definitively conclude that PDGFRβ$^+$ precursors differentiate into SCMFs, it does show a role for PDGFRβ$^+$ cells in alveolarisation. Whether this occurs via direct differentiation of SCMFs from PDGFRβ$^+$ precursors, or via paracrine signalling from PDGFRβ$^+$ cells is currently unknown.

Pdgfrb-Cre$^{+/-}$*;Gnaq*$^{fl/fl}$*;Gna11*$^{-/-}$ mouse lungs contained abnormal peripheral pulmonary vessels, with thickened vessel walls and reduced lumen diameter associated with muscularisation of the media (indicated by αSMA staining). These findings could be explained by pulmonary arterial hypertension (PAH), which could relate to hypoxaemia secondary to the profound pulmonary defects, in combination with disturbed GPCR signalling, resulting in vascular remodelling (Cheng et al., 2012; Patel et al., 2018). However, cardiac histology did not show thickening of the right ventricular wall in *Pdgfrb-Cre*$^{+/-}$*;Gnaq*$^{fl/fl}$*;Gna11*$^{-/-}$ mice, neither was any intimal or adventitial fibrosis observed, findings inconsistent with substantial PAH. A limitation of this study is that assessments such as the Fulton index to assess for right ventricular hypertrophy were not possible and so it is not possible to determine conclusively whether there was any PAH. An alternative explanation for the abnormal vasculature in *Pdgfrb-Cre*$^{+/-}$*;Gnaq*$^{fl/fl}$*;Gna11*$^{-/-}$ mice could be that altered activity of *Pdgfrb*-expressing cells influences vascular development or the growth, differentiation, and activity of constituent cells such as vascular smooth muscle cells. Furthermore, the observed increased lung weights in *Pdgfrb-Cre*$^{+/-}$*;Gnaq*$^{fl/fl}$*;Gna11*$^{-/-}$ mice could be linked to interstitial oedema and cardiac malfunction. However, it is not currently possible to define the precise cause of the vascular abnormalities observed.

Altered CMS-induced TGFβ activation is likely to be a key driver of the lung phenotypes observed in *Pdgfrb-Cre*$^{+/-}$*;Gnaq*$^{fl/fl}$*;Gna11*$^{-/-}$ and *Pdgfrb-Cre*$^{+/-}$*;Gnaq*$^{fl/fl}$*;Gna11*$^{-/-}$ mice. TGFβ drives myofibroblast differentiation, cellular migration, and ECM protein production (Harrell et al., 2018), and deficiencies and genetic polymorphisms in TGFβ signalling pathway components have been associated with emphysema (Bonniaud et al., 2004; Celedón et al., 2004; Hersh et al., 2009; Li et al., 2011). Both lung stretch and tightly-controlled TGFβ signalling are important for normal lung development and regeneration (Alejandre-Alcázar et al., 2008; Belcastro et al., 2015; Bonniaud et al., 2004; Chen et al., 2005; Chen et al., 2008; Deng et al., 2019; Donahoe et al., 2016; Gauldie et al., 2003; Nakanishi et al., 2007; Pieretti et al., 2014; Sterner-Kock et al., 2002; Vicencio et al., 2004), and CMS has been

Development • Accepted manuscript

demonstrated to induce TGFβ signalling in a number of models and organ systems (Froese et al., 2016; Fujita et al., 2010; Furumatsu et al., 2013; John et al., 2016; Maeda et al., 2011; Russo et al., 2018; Wang et al., 2013). Using the same *Gnaq*$^{fl/fl}$;*Gna11*$^{-/-}$ mice used in our study, John et al described age-related emphysema related to reduced stretch-induced TGFβ signalling in mice lacking $G_{\alpha q/11}$ in type II alveolar epithelial cells (John et al., 2016). Open access RNA-Seq data on the LungMAP and IPF Cell Atlas databases show that in human and mouse lung, PDGFRβ-positive cells include pericytes, fibroblasts and myofibroblasts (www.ipfcellatlas.com; www.lungmap.net). We therefore used human lung fibroblasts and murine embryonic fibroblasts to assess the role of mesenchymal $G_{\alpha q/11}$ in CMS-induced TGFβ signalling.

CMS-induced TGFβ signalling in HLFs and MEFs was dependent on serine proteases and independent of αv integrins, contrary to previous work in lung slices and epithelial cells (Froese et al., 2016; Xu et al., 2009). This indicated that TGFβ2, an isoform that is activated by proteases but not integrins (Jenkins, 2008), may be the primary TGFβ isoform activated by mesenchymal cell stretch. $G_{\alpha q/11}$-deficient human lung fibroblasts expressed less TGFβ2, but had unchanged levels of TGFβ1, compared with cells that express $G_{\alpha q/11}$, suggesting a TGFβ isoform-specific effect of $G_{\alpha q/11}$ deletion. These data suggest a novel pathway in which mesenchymal $G_{\alpha q/11}$ drives TGFβ2 production, which is then available for protease-mediated activation. While the use of MEFs and HLFs does not precisely recapitulate the fibroblast cell populations present during lung development, these data demonstrate conservation of stretch-induced TGFβ signalling in fibroblasts across species.

This is the first study to propose an isoform-specific role for TGFβ2 in mammalian alveolar development and lung homeostasis. The three TGFβ isoforms are highly expressed during lung development with distinct spatial and temporal expression patterns (Schmid et al., 1991), however little is known about the specific regulation of TGFβ2 signalling. *Tgfb2*$^{-/-}$ mice die shortly after birth from developmental abnormalities distinct from those seen in *Tgfb1*$^{-/-}$ or *Tgfb3*$^{-/-}$ mice (Kaartinen et al., 1995; Sanford et al., 1997; Shull et al., 1992). *Tgfb2*$^{-/-}$ mice have no gross lung morphological abnormalities in late intrauterine gestation, however collapsed conducting airways are found postnatally (Sanford et al., 1997). While the *Pdgfrb-Cre*$^{+/-}$;*Gnaq*$^{fl/fl}$;*Gna11*$^{-/-}$ mice generated in the present study did not share phenotypic features with*Tgfb2*$^{-/-}$ mice, it is possible that TGFβ2 production by non-mesenchymal cells is sufficient for normal prenatal development. Additionally, as alveolarisation occurs entirely postnatally in mice, the role of TGFβ2 in alveolar development that we describe could not be observed in *Tgfb2*$^{-/-}$ mice due to perinatal death. Our data demonstrate that loss of mesenchymal $G_{\alpha q/11}$ causes a loss of the precise control of TGFβ signalling in the lungs, resulting in abnormal alveologenesis and loss of lung homeostasis in developed lungs.

Development • Accepted manuscript

Further work is required to understand the precise roles of individual TGFβ isoforms in these processes.

The PDGF family is known be important in lung development and regeneration, with PDGFA being particularly important in alveolar development (Gokey et al., 2021; Gouveia et al., 2018; Gouveia et al., 2020). We found a trend towards reduced *Pdgfa* expression in MEFs with $G_{\alpha q/11}$ deletion, as well as *Pdgfb* and *Pdgfc*, suggesting that $G_{\alpha q/11}$ signalling may interact with PDGF-related pathways. Postnatal deletion of *Pdgfra*, which encodes the major receptor for PDGFA, reduces lung *Tgfb2*, but not *Tgfb1,* transcripts (Li et al., 2019), further supporting a role for PDGF signalling in $G_{\alpha q/11}$- and TGFβ2-driven alveolar development and regeneration. However, elastin deposition during alveologenesis may not be dependent on PDGFA (Gouveia et al., 2020), therefore PDGF-independent pathways are also likely to be involved in driving the abnormalities in *Pdgfrb-Cre*$^{+/-}$*;Gnaq*$^{fl/fl}$*;Gna11*$^{-/-}$ and *Pdgfrb-Cre/ERT2*$^{+/-}$*;Gnaq*$^{fl/fl}$*;Gna11*$^{-/-}$ mouse lungs. As pulmonary mesenchymal cells are predominantly PDGF receptor-expressing, rather than PDGF ligand producing (Gouveia et al., 2017), and $G_{\alpha q/11}$ deletion did not alter *Pdgfra* or *Pdgfrb* expression, we hypothesise that mesenchymal $G_{\alpha q/11}$ deletion reduces lung TGFβ2 signalling, which subsequently alters PDGF ligand expression by other cell types. However, it was beyond the scope of this work to dissect the interactions between $G_{\alpha q/11}$, TGFβ2, and PDGF signalling.

As PDGFRβ is a mesenchymal cell marker found outside of the lung, the other organs of *Pdgfrb-Cre*$^{+/-}$*;Gnaq*$^{fl/fl}$*;Gna11*$^{-/-}$ and *Pdgfrb-Cre/ERT2*$^{+/-}$*;Gnaq*$^{fl/fl}$*;Gna11*$^{-/-}$ mice were examined histologically. *Pdgfrb-Cre*$^{+/-}$*;Gnaq*$^{fl/fl}$*;Gna11*$^{-/-}$ kidneys demonstrated expansion and prominence of medullary mesenchymal cells. However, the kidneys of *Pdgfrb-Cre/ERT2*$^{+/-}$*;Gnaq*$^{fl/fl}$*;Gna11*$^{-/-}$ mice were normal, supporting the hypothesis that abnormalities observed in *Pdgfrb-Cre*$^{+/-}$*;Gnaq*$^{fl/fl}$*;Gna11*$^{-/-}$ kidneys were developmental in nature.

There are a number of limitations of this study. The poor condition of *Pdgfrb-Cre*$^{+/-}$*;Gnaq*$^{fl/fl}$*;Gna11*$^{-/-}$ mice limited the analyses to a single time point and precluded the study of CMS in vivo. The absence of detailed lineage tracing or single cell RNA sequencing of the *Pdgfrb-Cre*$^{+/-}$*;Gnaq*$^{fl/fl}$*;Gna11*$^{-/-}$ mouse lungs means it cannot be confirmed that the abnormalities were driven by any particular mesenchymal cell subtype. *Pdgfrb-Cre*$^{+/-}$ mice have been used to investigate the role of pericytes in various organ development and disease models (Diéguez-Hurtado et al., 2019; Eilken et al., 2017; Foo et al., 2006; Gong et al., 2018; He et al., 2020; Henderson et al., 2013; Ivanova et al., 2021; Wang et al., 2017; Zaitoun et al., 2019; Zhang et al., 2021), including a study that used a GFP reporter mouse to demonstrate *Pdgfrb-Cre*-induced gene recombination in lung pericytes during timepoints relevant to alveolarisation (Kato et al., 2018). However previous studies have shown that *Pdgfrb-Cre*-induced gene recombination can occur in other cell types, including

Development • Accepted manuscript

myofibroblasts induced by injury, fibroblasts, smooth muscle cells, and renal interstitial cells (Cuttler et al., 2011; Gong et al., 2018; Henderson et al., 2013; Schiessl et al., 2018; Ulvmar et al., 2016; Wang et al., 2019; Zou et al., 2018). Furthermore, *Pdgfrb* expression may vary at different stages of organ development and cellular differentiation (Salter et al., 2019), and it is possible that altered gene expression in a *Pdgfrb*-expressing precursor cell could influence the characteristics of non-*Pdgfrb*-expressing cells that derive from them. Therefore, while we hypothesise that abnormalities in pericyte activity, differentiation and migration underlie the defective alveologenesis and emphysema in mesenchymal $G_{\alpha q/11}$ knockout mice, the role of other mesenchymal cells in this process cannot be ruled out. However, we can conclude that $G_{\alpha q/11}$ signalling in *Pdgfrb*-expressing cells is important in lung development and homeostasis.

The growth restriction of *Pdgfrb-Cre*$^{+/-}$*;Gnaq*$^{fl/fl}$*;Gna11*$^{-/-}$ mice may indicate a nutritional deficiency that could have contributed to delayed alveolar development. While these animals did have renal abnormalities which may have contributed to the poor condition and failure to thrive of *Pdgfrb-Cre*$^{+/-}$*;Gnaq*$^{fl/fl}$*;Gna11*$^{-/-}$ mice, the bowel appeared normal and mice with mesenchymal $G_{\alpha q/11}$ deletion induced in adulthood had normal kidneys. This suggests a true pulmonary phenotype in mesenchymal $G_{\alpha q/11}$ knockout mice. Additionally, our in vitro data provide compelling evidence for a role for mesenchymal $G_{\alpha q/11}$ in a key lung developmental signalling pathway, suggesting that mesenchymal $G_{\alpha q/11}$ deletion generates a true lung developmental phenotype.

Finally, this study has not investigated the role of lung inflammation in mesenchymal $G_{\alpha q/11}$ knockout mice. TGFβ regulates inflammation, and John et al showed that emphysema in mice with a type II epithelial $G_{\alpha q/11}$ deletion was associated with lung inflammation and M2 macrophage polarisation (John *et al.*, 2016). The mononuclear cellular aggregates in the lungs of mice with mesenchymal $G_{\alpha q/11}$ deletion induced in adulthood could indicate abnormal inflammation in these mice. However, these cellular aggregates were not observed in mice with a germline mesenchymal $G_{\alpha q/11}$ knockout, and it was not possible to fully define the role of inflammation and the immune response in the emphysema observed in *Pdgfrb-Cre/ERT2*$^{+/-}$*;Gnaq*$^{fl/fl}$*;Gna11*$^{-/-}$ mice in our study.

In conclusion, this is the first study to generate mesenchymal $G_{\alpha q/11}$ deleted mice, and has demonstrated a novel signalling pathway for CMS-induced TGFβ2 signalling in murine embryonic and mature human mesenchymal cells that is important for alveologenesis and maintenance of the normal lung. These findings could have implications for the treatment of several conditions associated with dysregulated developmental and repair pathways, including fibrosis and emphysema.

Development • Accepted manuscript

Materials and Methods

Resource Availability

Lead Contact

Further information and requests for resources and reagents should be directed to and will be fulfilled by the Lead Contact, Amanda Goodwin (Amanda.Goodwin@nottingham.ac.uk).

Materials Availability

This study did not generate new unique reagents.

Data and Code Availability

This study did not analyse or generate any new datasets or code

Experimental Model and Subject Details

Animal Studies

Husbandry

Mice were housed under specific pathogen-free conditions, with standard food and water available *ad libitum*. All animal experiments were performed in accordance with the Animals (Scientific Procedures) Act 1986, and approved by the Animal Welfare and Ethical Review Board at the University of Nottingham.

Development • Accepted manuscript

Breeding strategy

For the germline mouse studies, mice with floxed alleles for *Gnaq* and germline deficiency in *Gna11* (*Gnaq*$^{fl/fl}$;*Gna11*$^{-/-}$) were crossed with mice that express Cre recombinase under the control of the *Pdgfrb* gene (*Pdgfrb-Cre*$^{+/-}$). *Pdgfrb-Cre*$^{+/-}$;*Gnaq*$^{+/fl}$;*Gna11*$^{+/-}$ offspring from this F1 generation were then bred with *Gnaq*$^{fl/fl}$;*Gna11*$^{-/-}$ founders to produce an F2 generation, including *Pdgfrb-Cre*$^{+/-}$;*Gnaq*$^{fl/fl}$;*Gna11*$^{-/-}$ mice. The genetic background for all mice was predominantly C57BL6, with a minimum of a six backcross generations. The generation of *Gnaq*$^{fl/fl}$;*Gna11*$^{-/-}$ and *Pdgfrb-Cre*$^{+/-}$ mice has been described previously (Foo et al., 2006; Offermanns et al., 1998; Wettschureck et al., 2001).

For the tamoxifen-inducible mouse gene knockout studies, the same breeding strategy was used as for the germline studies but substituting *Pdgfrb-Cre/ERT2*$^{+/-}$ mice (Jackson Laboratories) for *Pdgfrb-Cre*$^{+/-}$ animals. The generation of these mice has been described elsewhere (Gerl et al., 2015).

Genotyping

Mice were genotyped using DNA isolated from ear notch biopsies by PCR analysis with allele-specific primers (Eurofins). Primer sequences: *Cre* transgene 5'- GCG GTC TGG CAG TAA AAA CTA TC – 3', 5' - GTG AAA CAG CAT TGC TGT CAC TT – 3' (product 100bp); internal positive control 5' - CTA GGC CAC AGA ATT GAA AGA TCT – 3', 5' - GTA GGT GGA AAT TCT AGC ATC ATC C – 3' (product 324bp); *Gna11* wild-type 5' – AGC ATG CTG TAA GAC CGT AG - 3', 5' – GCC CCT TGT ACA GAT GGC AG – 3' (product 820bp); *Gna11* knockout 5' - CAG GGG TAG GTG ATG ATT GTG – 3', 5' – GAC TAG TGA GAC GTG CTA CTT CC - 3' (product 450bp); *Gnaq* wild-type and floxed alleles 5' – GCA TGC GTG TCC TTT ATG TGA G 3', 5' – AGC TTA GTC TGG TGA CAG AAG – 3' (products: 600bp (wild type), 700bp (floxed). For *Cre-ERT2*, the following primers were used: 5'- GAA CTG TCA CCG GGA GGA - 3', 5' - AGG CAA ATT TTG GTG TAC GG – 3' (400bp product).

PCR products were analysed by electrophoresis on ethidium bromide-stained agarose gels.

Mice were genotyped at 2 weeks old (P14). Genotype ratios of F2 mice from the *Gnaq*$^{fl/fl}$;*Gna11*$^{-/-}$ and *Pdgfrb-Cre*$^{+/-}$ crosses were compared with the expected Mendelian frequency (12.5% per genotype). Similarly, Genotype ratios of F2 mice from the *Gnaq*$^{fl/fl}$;*Gna11*$^{-/-}$ and *Pdgfrb-Cre/ERT2*$^{+/-}$ crosses were assessed, with an expected frequency of 5% for each Cre-expressing genotype.

Development • Accepted manuscript

Human Cells

For in vitro experiments using human lung fibroblasts, cells from 4-6 donors were used per group. Cells were used at passage 5-6 for all in vitro experiments.

Human lung fibroblasts (HLFs) were isolated from donated post-mortem or surgical lung biopsy samples, from male and female donors with and without pulmonary fibrosis. For non-fibrotic fibroblasts, cells were isolated from regions of lung distant from the area of primary diagnosis. Tissue was cut into 1mm x 1mm pieces and placed 10mm apart in a 10cm cell culture dish. Tissue was cultured in DMEM supplemented with 10% foetal calf serum (FCS, Fisher), L-glutamine (4mM, G7513, Sigma), penicillin (200 units/ml) and streptomycin (0.2mg/ml) (P4458, Sigma), and amphotericin B (2.5µg/ml, Cat# A2942, Sigma). Fibroblast outgrowth could be seen after 6-8 days. Tissue was removed from the cell culture dish if it became detached, or when cells had reached 80% confluency and were ready for passage. Cells were maintained in a humidified incubator at 37^{o}C, 5% CO_2/ 95% air, in Dulbecco's Modified Eagle's Medium (DMEM, Sigma), supplemented with 10% foetal calf serum (FCS, Fisher), L-glutamine (4mM, Sigma), penicillin (100 units/ml, Sigma) and streptomycin (0.1mg/ml, Sigma).

Murine Cells

Wild-type, *Gna12*$^{-/-}$*;Gna13*$^{-/-}$, and *Gnaq*$^{-/-}$*;Gna11*$^{-/-}$ murine embryonic fibroblasts (MEFs) were a gift from Prof Stefan Offermanns, and their generation has been described elsewhere (Gu et al., 2002; Zywietz et al., 2001). *Gnaq*, *Gna11*, *Gna12*, and *Gna13* gene expression was also confirmed in house prior to these studies. Cells were maintained in a humidified incubator at 37^{o}C, 5% CO_2/ 95% air, in Dulbecco's Modified Eagle's Medium (DMEM, Sigma), supplemented with 10% foetal calf serum (FCS, Fisher), L-glutamine (4mM, Sigma), penicillin (100 units/ml, Sigma) and streptomycin (0.1mg/ml, Sigma).

Method details

Mouse studies

Pdgfrb-Cre*$^{+/-}$*;Gnaq*$^{fl/fl}$*;Gna11*$^{-/-}$ *Mouse Phenotyping

Litters were observed for signs of ill health daily from birth. Mice were weighed at P14. Male and female mice were included in all analyses. Mice had not undergone any previous procedures. All mice that survived to P14 were phenotyped and had organs collected. Mouse phenotyping analyses were performed by an observer blinded to genotype. Genotype

Development • Accepted manuscript

information was not available to the phenotyping observer until all phenotyping and health status data had been recorded.

For comparisons, *Pdgfrb-Cre*$^{+/-}$;*Gnaq*$^{fl/fl}$;*Gna11*$^{-/-}$ (mesenchymal $G_{\alpha q/11}$ knockout mice) were compared to littermate *Pdgfrb-Cre*$^{-/-}$;*Gnaq*$^{fl/fl}$;*Gna11*$^{-/-}$ control mice (referred to as *Gna11*$^{-/-}$ controls).

Tamoxifen-inducible knockouts

Pdgfrb-Cre/ERT2$^{+/-}$;*Gnaq*$^{fl/fl}$;*Gna11*$^{-/-}$ offspring and their littermates were kept under standard conditions until 7 weeks of age (P49), when tamoxifen-containing chow (400mg/kg tamoxifen citrate, Envigo) was introduced *ad libitum*. Health scoring and weights were measured daily for 3 weeks as tamoxifen was administered. Animals were humanely killed after 3 weeks of tamoxifen administration (at 10 weeks old, P70).

For comparisons, *Pdgfrb-Cre/ERT2*$^{+/-}$;*Gnaq*$^{fl/fl}$;*Gna11*$^{-/-}$ (tamoxifen-inducible mesenchymal $G_{\alpha q/11}$ knockout mice) were compared to littermate *Pdgfrb-Cre/ERT2*$^{-/-}$;*Gnaq*$^{fl/fl}$;*Gna11*$^{-/-}$ control mice (referred to as *Gna11*$^{-/-}$ controls).

Organ Collection

Mice were humanely killed by intraperitoneal injection of pentobarbital, and organs collected for histological analyses. The lungs were perfused by injecting 40units/ml heparin sodium in PBS (Wockhardt) into the right ventricle, and inflated by cannulating the trachea and filling the lungs with 10% formalin (VWR) under gravity. The trachea was ligated, and the heart and lungs removed en bloc. Livers and kidneys were also collected. Organs were kept in 10% formalin (VWR) for 24 hours before paraffin embedding and sectioning.

Tissue histology staining

3µm (lung, kidney), and 5µm (heart, liver) formalin-fixed paraffin embedded tissue sections were deparaffinised in xylene and rehydrated in graded alcohols. Haematoxylin and eosin, Verhoeff van Gieson (elastin), and picrosirius red staining were performed as per standard protocols using buffers and stains prepared in house and mounted in DPX.

Staining solutions made in house

The following histology solutions were generated in house: Weigert's iodine (2g potassium iodide (Cat# 03124, Sigma), 1g iodine (Cat# 326143, Sigma), 100ml distilled water); Verheoff's solution (20ml 5% alcoholic haematoxylin (Cat# H3136, Sigma), 8ml 10% ferric chloride (Cat# 157740, Sigma), 8ml Weigert's iodine); Van Gieson's solution (5ml aqueous acid fuschin (Cat# F8129, Sigma), 100ml saturated aqueous picric acid (Cat# 84512.260, VWR)); Picro-sirius red solution (0.5g Direct Red 80 (Cat# 365548, Sigma), 500ml saturated

Development • Accepted manuscript

aqueous picric acid (Cat# 84512.260, VWR)); Weigert's haematoxylin (1:1 ratio of Weigert's solution A and Weigert's solution B); Weigert's solution A (1% haematoxylin (Cat# H3136, Sigma) in 100% ethanol); Weigert's solution B (4ml 30% ferric chloride (Cat# 157740, Sigma), 1ml 12N hydrochloric acid, 95ml water); Acidified water (5ml glacial acetic acid, 1l distilled water); Acid/alcohol solution (70% ethanol, 0.1% hydrochloric acid).

Haematoxylin and eosin (H&E) stain

After being deparaffinised and rehydrated, tissue sections were submerged in Mayers haematoxylin (Cat# S1275, Sigma) for 2 minutes, acid/alcohol solution for 1 minute, then 1% eosin solution (Cat# 101411-524, VWR) for 3 minutes. Sections were rinsed with tap water between each step, then dehydrated and mounted.

Elastin (Verhoeff Van Gieson) stain

Lung sections were deparaffinised and hydrated to distilled water, then stained in Verhoeff's solution for 1 hour until the tissue was completely black. Sections were differentiated in 2% ferric chloride (Cat# 157740, Sigma) until elastin foci were seen on a grey background, incubated in 5% sodium thiosulphate (Cat# 72049, Scientific Laboratory Supplies) for 1 minute, and then washed in running tap water for 5 minutes. Sections were then counterstained in Van Gieson's solution for 5 minutes, dehydrated and mounted as above.

Picrosirius red stain

Lung, kidney, and heart sections were deparaffinised and hydrated. Nuclei were stained with Weigert's haematoxylin for 8 minutes, and then washed in running tap water for 5 minutes. Sections were incubated in picrosirius red for 1 hour, washed in two changed of acidified water, then dehydrated and mounted.

Immunostaining

Tissue sections were deparaffinised in xylene and rehydrated in graded alcohols. Heat-mediated antigen retrieval was performed by boiling sections in a microwave for 20 minutes in 10mM citric acid buffer (pH 6.0). Endogenous peroxidase activity was blocked by incubating sections in 3% hydrogen peroxide in methanol for 30 minutes. Nonspecific binding was blocked with 5% goat serum (Cat# G9023, Sigma) in 0.1% BSA/PBS. Sections were incubated with primary antibody in 5% goat serum overnight at 4^{o}C in a humidified chamber, followed by incubations for 60 minutes with secondary antibody and 30 minutes with avidin-biotin complex (Cat# SP2001, Vector). Sections were then stained with diaminobenzidine (SIGMAFAST, Cat# D4418, Sigma), counterstained with Mayers

Development • Accepted manuscript

haematoxylin (Cat# S1275, Sigma), and mounted in DPX (Cat# 06522, Sigma). Slides were washed in PBS (Sigma) between incubation steps.

The following antibodies were used for immunohistochemistry: Rabbit anti-αSMA (Abcam, ab5694; 1:500), rabbit anti-CD31 (Abcam, ab182981; 1:2000), rabbit anti-ki67 (Abcam, ab15580; 1µg/ml), rabbit anti-pro-surfactant protein C (Sigma, Ab3786; 1:2000), rabbit anti-TGFβ2 (Proteintech, 19999-1-AP; 1:3000), rabbit anti-elastin (Atlas, HPA056941; 1:100), and biotinylated goat anti-rabbit IgG (Vector, BA1000; 1:200).

Image Quantification

Image acquisition

Images of H&E, elastin, and IHC were taken using a Nikon 90i microscope and NIS-Elements software v3.2 (Nikon). Polarised light imaging of picrosirius red stained samples was performed using a Zeiss Axioplan microscope (Zeiss) and MicroManager 1.4 software (Vale Lab, UCSF).

Staining quantification

For all analyses of histology images, *Pdgfrb-Cre*$^{+/-}$ *;Gnaq*$^{fl/fl}$*;Gna11*$^{-/-}$ or *Pdgfrb-Cre/ERT2*$^{+/-}$ *;Gnaq*$^{fl/fl}$*;Gna11*$^{-/-}$ mice were compared with *Pdgfrb-Cre*$^{-/-}$*;Gnaq*$^{fl/fl}$*;Gna11*$^{-/-}$ or *Pdgfrb-Cre/ERT2*$^{-/-}$ *;Gnaq*$^{fl/fl}$*;Gna11*$^{-/-}$ littermate controls (labelled as *Gna11*$^{-/-}$ controls), respectively. For histological analyses, four animals per genotype were assessed to allow differences in histological appearances to be detected. All image quantification was performed by an observer blinded to genotype. This observer was not unblinded to genotype until all image quantification data had been recorded.

For quantitative analyses of the lungs, 5-10 images were assessed per set of lungs, covering all lobes and avoiding major airways and central blood vessels. All morphometric analyses were performed using NIS Elements software v3.2 (Nikon), with the exception of peripheral pulmonary vessel thickness measurements and kidney measurements, which were performed using CaseViewer 2.3 software (3D Histech).

For quantification of immunohistochemistry and elastin staining, the “count” feature of ImageJ (NIH) was used. Elastin foci were identified as black fibres on VVG stain, and secondary crests were elastin positive if they had black staining that was not clearly a cell nucleus on Verhoeff van Geison staining. For immunohistochemistry staining, a cell was counted if it stained brown. Only nuclear DAB staining was counted for Ki67 quantification. For αSMA quantification, the number of αSMA-positive secondary crests per 40 x field was counted. For Ki67 and pro-SPC staining, the total number of cells per 40x field was

Development • Accepted manuscript

quantified by counting nuclei, and the proportion of Ki67 or pro-SPC positive cells calculated by dividing the number of stained cells per image by the total number of cells per image.

For quantification of TGFβ2 staining, the following scoring system was used and 7 fields (20x magnification) per mouse were analysed:

- **Score 0**: No cells stained.
- **Score 0.5**: 1-25 cells stained at low intensity
- **Score 1.0**: 1-25 cells stained at high intensity
- **Score 1.5**: 26-50 cells stained at low intensity
- **Score 2.0**: 26-50 cells stained at high intensity
- **Score 2.5**: >50 cells stained at low intensity
- **Score 3.0**: >50 cells stained at high intensity

Morphometry

Mean linear intercept (MLI) analysis of airspace size was performed as previously described (John et al., 2016). Briefly, 10x magnification images were overlaid with a grid comprised of 100μm squares, and “intercepts” between gridlines and airspace walls counted. The MLI was calculated by dividing the length of each gridline was divided by the intercept count. For alveolar wall thickness measurements, 40x magnification images were overlaid with five equally spaced horizontal lines and the alveolar wall thickness measured at points where lung tissue crossed each line using the “measure” function of NIS Elements. Mean MLI and alveolar wall thickness values were calculated for each mouse from all measurements across all images and data presented as median ± interquartile range. For secondary crest counts, 10x magnification images were used and secondary crests counted for each image.

For peripheral vessel wall thickness, ten random peripheral pulmonary vessels per mouse were identified as circular structures lined with a CD31-positive endothelial layer. The “measure” function of CaseViewer was used to measure the external and internal vessel diameters. The external vessel diameter (ED) was defined as the distance from the outermost aspect of the external wall of a vessel to the outermost aspect of the opposite wall, traversing the centre of the vessel lumen. The internal vessel diameter (ID) was defined as the distance from the innermost aspect of the vessel wall to the innermost aspect of the opposite vessel wall, traversing the centre of the vessel lumen. The following equations were used to calculate the vessel wall thickness (VWT) and internal vessel lumen diameter relative to total vessel diameter;

$$VWT = (ED-ID) / ED$$

$$\text{Internal vessel diameter} = ID / ED$$

Development • Accepted manuscript

For assessment of right ventricular hypertrophy, the left and right cardiac ventricular wall thickness was measured using CaseViewer, and the right: left ventricular wall thickness ratio calculated.

Breathing-related cyclical stretch experiments

Cells were seeded at 2 x 10^5 cells per well on collagen I-coated Bioflex® 6 well culture plates (Cat# 3001-C, Dunn Labortechnik) in DMEM supplemented with 10% FCS, L-glutamine (4mM), penicillin (100 units/ml) and streptomycin (0.1mg/ml) and allowed to adhere for 24 hours. The culture medium was changed to 1% FCS in DMEM with 4mM L-glutamine for 24 hours before stretching commenced. The Flexcell® FX-5000T system (Flexcell International Corporation) was used to apply cyclical stretch to cells in vitro, according to the manufacturer's instructions. MEFs were stretched at a frequency of 1Hz, and HLFs at 0.3Hz to mimic breathing in the relevant organism. 15% elongation and a sine waveform were used for all cyclical stretch experiments. Cyclical stretch was applied for 48 hours, except for experiments using siRNA-induced *GNAQ* and *GNA11* knockdown, where 24 hours of cyclical stretch was used. Unstretched control cells were cultured in identical conditions alongside the Flexcell® apparatus. Cells were lysed in protein lysis buffer (Cat# 9803, Cell Signalling Technology) supplemented with phosphatase (Phos-Stop, Cat# 04906837001, Sigma) and protease (Complete Mini, Cat# 04693124001, Sigma) inhibitors, and 20µM PMSF in isopropanol (Cat# P7626, Sigma). All experimental replicates were performed independently.

Chemical Inhibitors used in Cyclical Stretch System

When used, inhibitor compounds were applied in DMEM supplemented with 1% FCS and 4mM L-glutamine 30 minutes before stretching commenced. The activin receptor-like kinase (ALK5)/ type I TGFβ-receptor kinase inhibitor SB-525334 (Cat# S8822, Sigma) was used at a concentration of 50µM. A ROCK inhibitor (Y27632, Cat# Y0503, Sigma), pan-αv integrin inhibitor (CWHM-12, a gift from Dr David Griggs (St Louis University, Missouri, USA)), β1 integrin inhibitor (NOTT199SS, a gift from Dr Thomas McInally (University of Nottingham, UK)) matrix metalloproteinase (MMP) inhibitor GM6001 (Cat# CC1010, Sigma), and serine protease inhibitor AEBSF (Cat# SBR00015, Sigma) were used at varying concentrations. Where inhibitors were dissolved in DMSO, the negative control cells were treated with a DMSO concentration equivalent to that used in the highest inhibitor concentration.

GNAQ and GNA11 siRNA

SiRNAs for human *GNAQ* (ON-TARGET-plus SMARTpool GNAQ, Cat# L-008562-00-0005, Dharmacon) and *GNA11* (ON-TARGET-plus SMARTpool GNA11, Cat# L-010860-00-0005,

Development • Accepted manuscript

Dharmacon) were used to induce *GNAQ* and *GNA11* knockdown. A non-targeting siRNA pool was used as a control (ON-TARGET-plus non-targeting pool, Cat# D-001810-10-05, Dharmacon).

Cells were seeded at 1.5 x 10^5 cells per well of a 6 well collagen I-coated Bioflex® 6 well culture plates (Cat# 3001-C, Dunn Labortechnik) in antibiotic-free DMEM supplemented with 10% FCS and 4mM L-glutamine. The following day, *GNAQ* and *GNA11* siRNA was applied at a concentration of 15nM each with 4µl/ml DharmaFECT 1 transfection reagent (Cat# T-2001-01, Dharmacon) as per the manufacturer's protocol. At 48 hours after transfection, the media was changed to DMEM supplemented with 1% FCS and 4mM L-glutamine. Cyclical stretch was applied for 24 hours from 72 hours post-transfection. $G_{\alpha q/11}$ knockdown was confirmed by western blot and qPCR

Western blotting

Protein concentrations were determined by BCA assay using a commercially available kit (Cat# PN23227, ThermoFisher), according to the manufacturer's instructions. Equal amounts of protein (15-25µg) were loaded per lane of a 10% SDS-polyacrylamide gel and subject to electrophoresis, and transferred onto a polyvinylidene fluoride membrane (Cat# 1620177, BioRad). Membranes were blocked for 1 hour in either 5% non-fat milk (pSmad2, Smad2/3, αSMA, $G_{\alpha q}$, $G_{\alpha 11}$, GAPDH) or 3% BSA (TGFβ1, TGFβ2) in tris-buffered saline containing 0.1% Tween, pH 7.4 (TBST). Membranes were incubated overnight at 4^{O}C in blocking buffer with the appropriate primary antibody. Membranes were washed in TBST, then incubated for 1-2 hours in the appropriate HRP-conjugated secondary antibody in blocking buffer. Western blots were analysed using chemilluminescence and exposure to film (Cat# 28-9068-35, GE Healthcare). Where membranes were probed for two different proteins of the same molecular weight, i.e. pSmad2 and Smad2, the membrane was stripped after analysis of pSmad2 using Western Restore Stripping Buffer (Cat# 21059, Thermo-Fisher) for 5 minutes and re-blocked with 5% non-fat milk before application of the second primary antibody.

The following antibodies were used for western blots: Rabbit anti-phospho-Smad2 (pSmad2) (Cell Signaling Technology, 3108; 1:1000), rabbit anti-Smad2/3 (Cell Signaling Technology, 3102; 1:1000), rabbit anti-αSMA (Abcam, ab5694; 0.5µg/ml), rabbit anti-GAPDH (Abcam, ab181603; 1:10,000), rabbit anti-TGFβ1 (ab92486; 4µg/ml), mouse anti-TGFβ2 (Abcam, ab36495; 1:1000), rabbit anti $G_{\alpha 11}$ (Abcam, ab153951; 1:1000), goat anti-$G_{\alpha q}$ (Abcam, ab128060; 0.1µg/ml), HRP-conjugated goat-anti-rabbit (Agilent, P044801-2; 1:3000), HRP-conjugated rabbit-anti-goat (Agilent, P016002-2; 1:3000), HRP-conjugated rabbit anti-mouse (Agilent, P0260022-2, 1:3000).

Development • Accepted manuscript

Densitometry Analysis of Western Blots

Densitometry was performed using ImageJ (National Institutes of Health) on scanned western blot images. JPEG images were converted into greyscale images, and the software used to calculate densitometry values for each band relative to the other bands. These relative densitometry values were used to calculate the expression of protein relative to loading control using the equation: Protein relative to loading control = protein densitometry value/ loading control protein densitometry value

Quantitative PCR

RNA was isolated from in vitro experiments using the Machery-Nagel Nucleospin RNA isolation kit (Cat# 740955.250) according to the manufacturer's instructions. Complementary DNA (cDNA) was reverse transcribed from 200µg RNA using Superscript IV Reverse Transcriptase (Cat# 18090050, Thermo Fisher) according to the manufacturer's protocol. Quantitative PCR was performed on cDNA using gene-specific primers (see below), and an MXPro3000 qPCR machine (Stratagene) at an annealing temperature of 60°C for 40 cycles. KAPA SYBR FastTaq (Cat# KK4618, Sigma) was used for qPCR of all genes other than *Pdgfa*, *Pdgfb*, *Pdgfc*, *Pdgfd*, *Pdgfra*, and *Pdgfrb*, for which PerfeCTa SYBR Green Fastmix (Cat# 733-1382, VWR) was used. Amplification of a single PCR product was confirmed by melting curve analysis. The delta-delta Ct method was used to quantify gene expression relative to the housekeeping genes *Hprt* (mouse samples) or *B2M* (human samples).

Primer were obtained from Eurofins. Sequences for mouse genes were: *Hprt* forward 5' – TGA AAG ACT TGC TCG AGA TGT CA - 3', *Hprt* reverse 5' CCA GCA GGT CAG CAA AGA ACT 3', *Acta2* forward 5' GGG ATC CTG ACG CTG AAG TA 3', *Acta2* reverse 5' GAC AGC ACA GCC TGA ATA GC 3', *Eln* forward 5' GAT GGT GCA CAC CTT TGT TG 3', *Eln* reverse 5' CAG TGT GAG CCA TCT CA 3', *Col1a1* forward 5' AGC TTT GTG CAC CTC CGG CT 3', *Col1a1* reverse 5' ACA CAG CCG TGC CAT TGT GG 3', *Col3a1* forward 5' TTT GCA GCC TGG GCT CAT TT 3', *Col3a1* reverse 5' AGG TAC CGA TTT GAA CAG ACT, *Pdgfa* forward 5' GAG ATA CCC CGG GAG TTG A 3', *Pdgfa* reverse 5' TCT TGC AAA CTG CAG GAA TG 3', *Pdgfb* forward 5' TGA AAT GCT GAG CGA CCA C 3', *Pdgfb* reverse 5' AGC TTT CCA ACT CGA CTC C 3', *Pdgfc* forward 5' AGG TTG TCT CCT GGT CAA GC 3', *Pdgfc* reverse 5' CCT GCG TTT CCT CTA CAC AC 3', *Pdgfd* forward 5'CCA AGG AAC CTG CTT CTG AC 3', *Pdgfd* reverse 5' CTT GGA GGG ATC TCC TTG TG 3', *Pdgfra*

Development • Accepted manuscript

forward 5’ CAA ACC CTG AGA CCA CAA TG 3’, *Pdgfra* reverse 5’ TCC CCC AAC AGT AAC CCA AG 3’, *Pdgfrb* forward TGC CTC AGC CAA ATG TCA CC 3’, *Pdgfrb* reverse 5’ TGC TCA CCA CCT CGT ATT CC 3’.

Primer sequences for human genes were: *GNAQ* forward 5’ – GGACAGGAGAGGGTGGCAAG – 3’, *GNAQ* reverse 5’ – TGGGATCTTGAGTGTGTCCA – 3’, *GNA11* forward 5’ – CCACTGCTTTGAGAACGTGA – 3’, *GNA11* reverse 5’ GCAGGTCCTTCTTGTTGAGG – 3’, *B2M* forward 5’AATCCAAATGCGGCATCT3’, *B2M* reverse 5’GAGTATGCCTGCCGTGTG3’.

Statistical Analyses

Statistical analyses were performed using GraphPad Prism 8.2 software (GraphPad). For experiments with group sizes of 5 or less, a non-parametric test was used. For experiments with group sizes of 6 or over, data were assessed for normality and a parametric test used if data followed a normal distribution.

Acknowledgements

We thank Dr Thomas McInally (University of Nottingham, UK) and Dr David Griggs (St Louis University, Missouri, USA) for supplying the compounds NOTT199SS and CWHM-12, respectively. NOTT199SS was identified as part of an MSci Chemistry undergraduate integrin drug discovery collaboration between the School of Chemistry at the University of Nottingham and GlaxoSmithKline (GSK), supervised by Dr Simon Macdonald (GSK) and Dr Thomas McInally (University of Nottingham). We also thank Dr Tim Kendall (University of Edinburgh), for his opinion on the liver histology.

We would also like to acknowledge the University of Nottingham Bio-Support and School of Life Sciences Imaging (SLIM) units for their support with the animal work and polarised light microscopy, respectively.

Declarations of Interests

RGJ reports grants or contracts from Astra Zeneca, Biogen, Galecto, GlaxoSmithKline, Nordic Biosciences, RedX, Plaint; consulting fees from Bristol Myers Squibb, Chiesi, Daewoong, GlaxoSmithKline, Veracyte, Resolution Therapeutics and Pliant; honoraria from Boehringer Ingelheim, Chiesi, Roch, PatientMPower, and AstraZeneca; payment for expert testimony from Pinsent Masons LLP; advisory or data monitoring roles with Boehringer Ingelheim, Galapagos, and Vicore; leadership role in NuMedii; President of Action for Pulmonary Fibrosis.

Development • Accepted manuscript

ATG, AEJ, CJ, AH, ALT, KS, MP, NCH, SO – no competing interests

Funding

This work was funded by a Medical Research Council Clinical Research Training Fellowship held by ATG (MR P001327/1). ATG was also funded by a National Institute for Health Research Academic Clinical Fellowship (2982) and a National Institute for Health Research Academic Clinical Lecturer post (CL-2020-12-003) for parts of this project. ALT was funded by a Medical Research Foundation fellowship (MRFAUK-2015-312) during this work. GJ is funded by a National Institute for Health Research Professorship (NIHR-RP-2017-08-ST2-014). NCH is supported by a Wellcome Trust Senior Research Fellowship in Clinical Science (219542/Z/19/Z).

Author contributions

ATG and GJ conceived project. ATG performed experiments, conducted image analysis, and wrote the original draft manuscript. AEJ supervised and gave methodological guidance for mouse phenotyping experiments and microscopy. CJ performed some of the immunohistochemistry included in this work. ATG, AEJ, AH, and ALT conducted animal monitoring and tissue collection. ALT established original cultures of human lung fibroblasts used in this study. KS and MP provided expert guidance on the performing and interpretation of kidney histology. NCH and SO provided and guided the breeding of *Pdgfrb-Cre*$^{+/-}$ and *Gnaq*$^{fl/fl}$;*Gna11*$^{-/-}$ mice, respectively. GJ supervised the entire project. All authors reviewed the original draft manuscript and contributed to editing and preparation of the final manuscript.

References

Alejandre-Alcázar, M. A., Michiels-Corsten, M., Vicencio, A. G., Reiss, I., Ryu, J., de Krijger, R. R., Haddad, G. G., Tibboel, D., Seeger, W., Eickelberg, O., et al. (2008). TGF-beta signaling is dynamically regulated during the alveolarization of rodent and human lungs. *Dev Dyn* **237**, 259-269.

Barron, L., Gharib, S. A. and Duffield, J. S. (2016). Lung Pericytes and Resident Fibroblasts: Busy Multitaskers. *Am J Pathol* **186**, 2519-2531.

Bartram, U. and Speer, C. P. (2004). The role of transforming growth factor beta in lung development and disease. *Chest* **125**, 754-765.

Development • Accepted manuscript

Beauchemin, K. J., Wells, J. M., Kho, A. T., Philip, V. M., Kamir, D., Kohane, I. S., Graber, J. H. and Bult, C. J. (2016). Temporal dynamics of the developing lung transcriptome in three common inbred strains of laboratory mice reveals multiple stages of postnatal alveolar development. *PeerJ* **4**, e2318.

Belcastro, R., Lopez, L., Li, J., Masood, A. and Tanswell, A. K. (2015). Chronic lung injury in the neonatal rat: up-regulation of TGFβ1 and nitration of IGF-R1 by peroxynitrite as likely contributors to impaired alveologenesis. *Free Radic Biol Med* **80**, 1-11.

Bonniaud, P., Kolb, M., Galt, T., Robertson, J., Robbins, C., Stampfli, M., Lavery, C., Margetts, P. J., Roberts, A. B. and Gauldie, J. (2004). Smad3 null mice develop airspace enlargement and are resistant to TGF-beta-mediated pulmonary fibrosis. *J Immunol* **173**, 2099-2108.

Boström, H., Willetts, K., Pekny, M., Levéen, P., Lindahl, P., Hedstrand, H., Pekna, M., Hellström, M., Gebre-Medhin, S., Schalling, M., et al. (1996). PDGF-A signaling is a critical event in lung alveolar myofibroblast development and alveogenesis. *Cell* **85**, 863-873.

Celedón, J. C., Lange, C., Raby, B. A., Litonjua, A. A., Palmer, L. J., DeMeo, D. L., Reilly, J. J., Kwiatkowski, D. J., Chapman, H. A., Laird, N., et al. (2004). The transforming growth factor-beta1 (TGFB1) gene is associated with chronic obstructive pulmonary disease (COPD). *Hum Mol Genet* **13**, 1649-1656.

Chanda, D., Otoupalova, E., Smith, S. R., Volckaert, T., De Langhe, S. P. and Thannickal, V. J. (2019). Developmental pathways in the pathogenesis of lung fibrosis. *Mol Aspects Med* **65**, 56-69.

Chen, H., Sun, J., Buckley, S., Chen, C., Warburton, D., Wang, X. F. and Shi, W. (2005). Abnormal mouse lung alveolarization caused by Smad3 deficiency is a developmental antecedent of centrilobular emphysema. *Am J Physiol Lung Cell Mol Physiol* **288**, L683-691.

Chen, H., Zhuang, F., Liu, Y. H., Xu, B., Del Moral, P., Deng, W., Chai, Y., Kolb, M., Gauldie, J., Warburton, D., et al. (2008). TGF-beta receptor II in epithelia versus mesenchyme plays distinct roles in the developing lung. *Eur Respir J* **32**, 285-295.

Cheng, H. Y., Dong, A., Panchatcharam, M., Mueller, P., Yang, F., Li, Z., Mills, G., Chun, J., Morris, A. J. and Smyth, S. S. (2012). Lysophosphatidic acid signaling protects pulmonary vasculature from hypoxia-induced remodeling. *Arterioscler Thromb Vasc Biol* **32**, 24-32.

Cuttler, A. S., LeClair, R. J., Stohn, J. P., Wang, Q., Sorenson, C. M., Liaw, L. and Lindner, V. (2011). Characterization of Pdgfrb-Cre transgenic mice reveals reduction of ROSA26 reporter activity in remodeling arteries. *Genesis* **49**, 673-680.

Dabovic, B., Robertson, I. B., Zilberberg, L., Vassallo, M., Davis, E. C. and Rifkin, D. B. (2015). Function of latent TGFβ binding protein 4 and fibulin 5 in elastogenesis and lung development. *J Cell Physiol* **230**, 226-236.

Development • Accepted manuscript

Deng, S., Zhang, H., Han, W., Guo, C. and Deng, C. (2019). Transforming Growth Factor-β-Neutralizing Antibodies Improve Alveolarization in the Oxygen-Exposed Newborn Mouse Lung. *J Interferon Cytokine Res* **39**, 106-116.

Diéguez-Hurtado, R., Kato, K., Giaimo, B. D., Nieminen-Kelhä, M., Arf, H., Ferrante, F., Bartkuhn, M., Zimmermann, T., Bixel, M. G., Eilken, H. M., et al. (2019). Loss of the transcription factor RBPJ induces disease-promoting properties in brain pericytes. *Nat Commun* **10**, 2817.

Dolhnikoff, M., Mauad, T. and Ludwig, M. S. (1999). Extracellular matrix and oscillatory mechanics of rat lung parenchyma in bleomycin-induced fibrosis. *American Journal of Respiratory & Critical Care Medicine* **160**, 1750-1757.

Donahoe, P. K., Longoni, M. and High, F. A. (2016). Polygenic Causes of Congenital Diaphragmatic Hernia Produce Common Lung Pathologies. *Am J Pathol* **186**, 2532-2543.

Eilken, H. M., Diéguez-Hurtado, R., Schmidt, I., Nakayama, M., Jeong, H. W., Arf, H., Adams, S., Ferrara, N. and Adams, R. H. (2017). Pericytes regulate VEGF-induced endothelial sprouting through VEGFR1. *Nat Commun* **8**, 1574.

Foo, S. S., Turner, C. J., Adams, S., Compagni, A., Aubyn, D., Kogata, N., Lindblom, P., Shani, M., Zicha, D. and Adams, R. H. (2006). Ephrin-B2 controls cell motility and adhesion during blood-vessel-wall assembly. *Cell* **124**, 161-173.

Froese, A. R., Shimbori, C., Bellaye, P. S., Inman, M., Obex, S., Fatima, S., Jenkins, G., Gauldie, J., Ask, K. and Kolb, M. (2016). Stretch-induced Activation of Transforming Growth Factor-beta1 in Pulmonary Fibrosis. *Am J Respir Crit Care Med* **194**, 84-96.

Fujita, H., Hida, M., Kanemoto, K., Fukuda, K., Nagata, M. and Awazu, M. (2010). Cyclic stretch induces proliferation and TGF-beta1-mediated apoptosis via p38 and ERK in ureteric bud cells. *Am J Physiol Renal Physiol* **299**, F648-655.

Funke, M., Knudsen, L., Lagares, D., Ebener, S., Probst, C. K., Fontaine, B. A., Franklin, A., Kellner, M., Kuhnel, M., Matthieu, S., et al. (2016). Lysophosphatidic Acid Signaling through the Lysophosphatidic Acid-1 Receptor Is Required for Alveolarization. *Am J Respir Cell Mol Biol* **55**, 105-116.

Furumatsu, T., Matsumoto, E., Kanazawa, T., Fujii, M., Lu, Z., Kajiki, R. and Ozaki, T. (2013). Tensile strain increases expression of CCN2 and COL2A1 by activating TGF-beta-Smad2/3 pathway in chondrocytic cells. *J Biomech* **46**, 1508-1515.

Gauldie, J., Galt, T., Bonniaud, P., Robbins, C., Kelly, M. and Warburton, D. (2003). Transfer of the active form of transforming growth factor-beta 1 gene to newborn rat lung induces changes consistent with bronchopulmonary dysplasia. *Am J Pathol* **163**, 2575-2584.

Development • Accepted manuscript

Gerl, K., Miquerol, L., Todorov, V. T., Hugo, C. P., Adams, R. H., Kurtz, A. and Kurt, B. (2015). Inducible glomerular erythropoietin production in the adult kidney. *Kidney Int* **88**, 1345-1355.

Gokey, J. J., Snowball, J., Green, J., Waltamath, M., Spinney, J. J., Black, K. E., Hariri, L. P., Xu, Y. and Perl, A. K. (2021). Pretreatment of aged mice with retinoic acid supports alveolar regeneration via upregulation of reciprocal PDGFA signalling. *Thorax* **76**, 456-467.

Gong, X., Guo, X., Huang, R., Liao, H., Zhang, Q., Yan, J., Luo, L., Qiu, A., Sun, Y. and Liang, X. (2018). Expression of ILK in renal stroma is essential for multiple aspects of renal development. *Am J Physiol Renal Physiol* **315**, F374-f385.

Gouveia, L., Betsholtz, C. and Andrae, J. (2017). Expression analysis of platelet-derived growth factor receptor alpha and its ligands in the developing mouse lung. *Physiol Rep* **5**.

---- (2018). PDGF-A signaling is required for secondary alveolar septation and controls epithelial proliferation in the developing lung. *Development* **145**.

Gouveia, L., Kraut, S., Hadzic, S., Vazquéz-Liébanas, E., Kojonazarov, B., Wu, C. Y., Veith, C., He, L., Mermelekas, G., Schermuly, R. T., et al. (2020). Lung developmental arrest caused by PDGF-A deletion: consequences for the adult mouse lung. *Am J Physiol Lung Cell Mol Physiol* **318**, L831-l843.

Gu, J. L., Muller, S., Mancino, V., Offermanns, S. and Simon, M. I. (2002). Interaction of G alpha(12) with G alpha(13) and G alpha(q) signaling pathways. *Proc Natl Acad Sci U S A* **99**, 9352-9357.

Harrell, C. R., Simovic Markovic, B., Fellabaum, C., Arsenijevic, A., Djonov, V. and Volarevic, V. (2018). Molecular mechanisms underlying therapeutic potential of pericytes. *J Biomed Sci* **25**, 21.

He, Q., Li, X., He, L., Li, Y., Betsholtz, C. and Welsh, M. (2020). Pericyte dysfunction due to Shb gene deficiency increases B16F10 melanoma lung metastasis. *Int J Cancer* **147**, 2634-2644.

Henderson, N. C., Arnold, T. D., Katamura, Y., Giacomini, M. M., Rodriguez, J. D., McCarty, J. H., Pellicoro, A., Raschperger, E., Betsholtz, C., Ruminski, P. G., et al. (2013). Targeting of alphav integrin identifies a core molecular pathway that regulates fibrosis in several organs. *Nat Med* **19**, 1617-1624.

Hersh, C. P., Hansel, N. N., Barnes, K. C., Lomas, D. A., Pillai, S. G., Coxson, H. O., Mathias, R. A., Rafaels, N. M., Wise, R. A., Connett, J. E., et al. (2009). Transforming growth factor-beta receptor-3 is associated with pulmonary emphysema. *Am J Respir Cell Mol Biol* **41**, 324-331.

Hilgendorff, A., Parai, K., Ertsey, R., Juliana Rey-Parra, G., Thebaud, B., Tamosiuniene, R., Jain, N., Navarro, E. F., Starcher, B. C., Nicolls, M. R., et al. (2012). Neonatal mice genetically modified to express the elastase inhibitor elafin are

Development • Accepted manuscript

protected against the adverse effects of mechanical ventilation on lung growth. *Am J Physiol Lung Cell Mol Physiol* **303**, L215-227.

Hoyer, D. P., Gronke, S., Frank, K. F., Addicks, K., Wettschureck, N., Offermanns, S., Erdmann, E. and Reuter, H. (2010). Diabetes-related defects in sarcoplasmic Ca2+ release are prevented by inactivation of G(alpha)11 and G(alpha)q in murine cardiomyocytes. *Mol Cell Biochem* **341**, 235-244.

Ito, J. T., Lourenço, J. D., Righetti, R. F., Tibério, I., Prado, C. M. and Lopes, F. (2019). Extracellular Matrix Component Remodeling in Respiratory Diseases: What Has Been Found in Clinical and Experimental Studies? *Cells* **8**.

Ivanova, E., Corona, C., Eleftheriou, C. G., Bianchimano, P. and Sagdullaev, B. T. (2021). Retina-specific targeting of pericytes reveals structural diversity and enables control of capillary blood flow. *J Comp Neurol* **529**, 1121-1134.

Jenkins, G. (2008). The role of proteases in transforming growth factor-beta activation. *Int J Biochem Cell Biol* **40**, 1068-1078.

Jesudason, R., Sato, S., Parameswaran, H., Araujo, A. D., Majumdar, A., Allen, P. G., Bartolak-Suki, E. and Suki, B. (2010). Mechanical forces regulate elastase activity and binding site availability in lung elastin. *Biophys J* **99**, 3076-3083.

John, A. E., Wilson, M. R., Habgood, A., Porte, J., Tatler, A. L., Stavrou, A., Miele, G., Jolly, L., Knox, A. J., Takata, M., et al. (2016). Loss of epithelial Gq and G11 signaling inhibits TGFbeta production but promotes IL-33-mediated macrophage polarization and emphysema. *Sci Signal* **9**, ra104.

Kaartinen, V., Voncken, J. W., Shuler, C., Warburton, D., Bu, D., Heisterkamp, N. and Groffen, J. (1995). Abnormal lung development and cleft palate in mice lacking TGF-beta 3 indicates defects of epithelial-mesenchymal interaction. *Nat Genet* **11**, 415-421.

Kato, K., Dieguez-Hurtado, R., Park, D. Y., Hong, S. P., Kato-Azuma, S., Adams, S., Stehling, M., Trappmann, B., Wrana, J. L., Koh, G. Y., et al. (2018). Pulmonary pericytes regulate lung morphogenesis. *Nat Commun* **9**, 2448.

Kiermayer, C., Conrad, M., Schneider, M., Schmidt, J. and Brielmeier, M. (2007). Optimization of spatiotemporal gene inactivation in mouse heart by oral application of tamoxifen citrate. *Genesis* **45**, 11-16.

Laboratory, Jackson. 029684 - B6.Cg-Tg(Pdgfrb-cre/ERT2)6096Rha/J (jax.org).

Li, C., Lee, M. K., Gao, F., Webster, S., Di, H., Duan, J., Yang, C. Y., Bhopal, N., Peinado, N., Pryhuber, G., et al. (2019). Secondary crest myofibroblast PDGFRα controls the elastogenesis pathway via a secondary tier of signaling networks during alveologenesis. *Development* **146**.

Development • Accepted manuscript

Li, C., Li, M., Li, S., Xing, Y., Yang, C. Y., Li, A., Borok, Z., De Langhe, S. and Minoo, P. (2015). Progenitors of secondary crest myofibroblasts are developmentally committed in early lung mesoderm. *Stem Cells* **33**, 999-1012.

Li, M., Krishnaveni, M. S., Li, C., Zhou, B., Xing, Y., Banfalvi, A., Li, A., Lombardi, V., Akbari, O., Borok, Z., et al. (2011). Epithelium-specific deletion of TGF-β receptor type II protects mice from bleomycin-induced pulmonary fibrosis. *J Clin Invest* **121**, 277-287.

Li, R., Bernau, K., Sandbo, N., Gu, J., Preissl, S. and Sun, X. (2018). Pdgfra marks a cellular lineage with distinct contributions to myofibroblasts in lung maturation and injury response. *Elife* **7**.

Lindahl, P., Karlsson, L., Hellström, M., Gebre-Medhin, S., Willetts, K., Heath, J. K. and Betsholtz, C. (1997). Alveogenesis failure in PDGF-A-deficient mice is coupled to lack of distal spreading of alveolar smooth muscle cell progenitors during lung development. *Development* **124**, 3943-3953.

Lovering, A. T., Elliott, J. E., Laurie, S. S., Beasley, K. M., Gust, C. E., Mangum, T. S., Gladstone, I. M. and Duke, J. W. (2014). Ventilatory and sensory responses in adult survivors of preterm birth and bronchopulmonary dysplasia with reduced exercise capacity. *Ann Am Thorac Soc* **11**, 1528-1537.

Maeda, T., Sakabe, T., Sunaga, A., Sakai, K., Rivera, A. L., Keene, D. R., Sasaki, T., Stavnezer, E., Iannotti, J., Schweitzer, R., et al. (2011). Conversion of mechanical force into TGF-beta-mediated biochemical signals. *Curr Biol* **21**, 933-941.

McGowan, S. E., Grossmann, R. E., Kimani, P. W. and Holmes, A. J. (2008). Platelet-derived growth factor receptor-alpha-expressing cells localize to the alveolar entry ring and have characteristics of myofibroblasts during pulmonary alveolar septal formation. *Anat Rec (Hoboken)* **291**, 1649-1661.

Mecham, R. P. (2018). Elastin in lung development and disease pathogenesis. *Matrix Biol* **73**, 6-20.

Mizikova, I. and Morty, R. E. (2015). The Extracellular Matrix in Bronchopulmonary Dysplasia: Target and Source. *Front Med (Lausanne)* **2**, 91.

Nakanishi, H., Sugiura, T., Streisand, J. B., Lonning, S. M. and Roberts, J. D., Jr. (2007). TGF-beta-neutralizing antibodies improve pulmonary alveologenesis and vasculogenesis in the injured newborn lung. *Am J Physiol Lung Cell Mol Physiol* **293**, L151-161.

Offermanns, S., Zhao, L. P., Gohla, A., Sarosi, I., Simon, M. I. and Wilkie, T. M. (1998). Embryonic cardiomyocyte hypoplasia and craniofacial defects in G alpha q/G alpha 11-mutant mice. *EMBO J* **17**, 4304-4312.

Development • Accepted manuscript

Pakshir, P., Noskovicova, N., Lodyga, M., Son, D. O., Schuster, R., Goodwin, A., Karvonen, H. and Hinz, B. (2020). The myofibroblast at a glance. *J Cell Sci* **133**.

Patel, J. A., Shen, L., Hall, S. M., Benyahia, C., Norel, X., McAnulty, R. J., Moledina, S., Silverstein, A. M., Whittle, B. J. and Clapp, L. H. (2018). Prostanoid EP_2 Receptors Are Up-Regulated in Human Pulmonary Arterial Hypertension: A Key Anti-Proliferative Target for Treprostinil in Smooth Muscle Cells. *Int J Mol Sci* **19**.

Pieretti, A. C., Ahmed, A. M., Roberts, J. D., Jr. and Kelleher, C. M. (2014). A novel in vitro model to study alveologenesis . *Am J Respir Cell Mol Biol* **50**, 459-469.

Pozarska, A., Rodriguez-Castillo, J. A., Surate Solaligue, D. E., Ntokou, A., Rath, P., Mizikova, I., Madurga, A., Mayer, K., Vadasz, I., Herold, S., et al. (2017). Stereological monitoring of mouse lung alveolarization from the early postnatal period to adulthood. *Am J Physiol Lung Cell Mol Physiol* **312**, L882-l895.

Ricard, N., Tu, L., Le Hiress, M., Huertas, A., Phan, C., Thuillet, R., Sattler, C., Fadel, E., Seferian, A., Montani, D., et al. (2014). Increased pericyte coverage mediated by endothelial-derived fibroblast growth factor-2 and interleukin-6 is a source of smooth muscle-like cells in pulmonary hypertension. *Circulation* **129**, 1586-1597.

Riccetti, M., Gokey, J. J., Aronow, B. and Perl, A. T. (2020). The elephant in the lung: Integrating lineage-tracing, molecular markers, and single cell sequencing data to identify distinct fibroblast populations during lung development and regeneration. *Matrix Biol* **91-92**, 51-74.

Russo, T. A., Stoll, D., Nader, H. B. and Dreyfuss, J. L. (2018). Mechanical stretch implications for vascular endothelial cells: Altered extracellular matrix synthesis and remodeling in pathological conditions. *Life Sci* **213**, 214-225.

Salter, D. M., Griffin, M., Muir, M., Teo, K., Culley, J., Smith, J. R., Gomez-Cuadrado, L., Matchett, K., Sims, A. H., Hayward, L., et al. (2019). Development of mouse models of angiosarcoma driven by p53. *Dis Model Mech* **12**.

Sanford, L. P., Ormsby, I., Gittenberger-de Groot, A. C., Sariola, H., Friedman, R., Boivin, G. P., Cardell, E. L. and Doetschman, T. (1997). TGFbeta2 knockout mice have multiple developmental defects that are non-overlapping with other TGFbeta knockout phenotypes. *Development* **124**, 2659-2670.

Sassmann, A., Gier, B., Grone, H. J., Drews, G., Offermanns, S. and Wettschureck, N. (2010). The Gq/G11-mediated signaling pathway is critical for autocrine potentiation of insulin secretion in mice. *J Clin Invest* **120**, 2184-2193.

Schiessl, I. M., Grill, A., Fremter, K., Steppan, D., Hellmuth, M. K. and Castrop, H. (2018). Renal Interstitial Platelet-Derived Growth Factor Receptor-β Cells Support Proximal Tubular Regeneration. *J Am Soc Nephrol* **29**, 1383-1396.

Schmid, P., Cox, D., Bilbe, G., Maier, R. and McMaster, G. K. (1991). Differential expression of TGF beta 1, beta 2 and beta 3 genes during mouse embryogenesis. *Development* **111**, 117-130.

Development • Accepted manuscript

Shull, M. M., Ormsby, I., Kier, A. B., Pawlowski, S., Diebold, R. J., Yin, M., Allen, R., Sidman, C., Proetzel, G., Calvin, D., et al. (1992). Targeted disruption of the mouse transforming growth factor-beta 1 gene results in multifocal inflammatory disease. *Nature* **359**, 693-699.

Sterner-Kock, A., Thorey, I. S., Koli, K., Wempe, F., Otte, J., Bangsow, T., Kuhlmeier, K., Kirchner, T., Jin, S., Keski-Oja, J., et al. (2002). Disruption of the gene encoding the latent transforming growth factor-beta binding protein 4 (LTBP-4) causes abnormal lung development, cardiomyopathy, and colorectal cancer. *Genes Dev* **16**, 2264-2273.

Suki, B., Jesudason, R., Sato, S., Parameswaran, H., Araujo, A. D., Majumdar, A., Allen, P. G. and Bartolak-Suki, E. (2012). Mechanical failure, stress redistribution, elastase activity and binding site availability on elastin during the progression of emphysema. *Pulm Pharmacol Ther* **25**, 268-275.

Ulvmar, M. H., Martinez-Corral, I., Stanczuk, L. and Mäkinen, T. (2016). Pdgfrb-Cre targets lymphatic endothelial cells of both venous and non-venous origins. *Genesis* **54**, 350-358.

Vicencio, A. G., Lee, C. G., Cho, S. J., Eickelberg, O., Chuu, Y., Haddad, G. G. and Elias, J. A. (2004). Conditional overexpression of bioactive transforming growth factor-beta1 in neonatal mouse lung: a new model for bronchopulmonary dysplasia? *Am J Respir Cell Mol Biol* **31**, 650-656.

Wang, B. W., Wu, G. J., Cheng, W. P. and Shyu, K. G. (2013). Mechanical stretch via transforming growth factor-beta1 activates microRNA-208a to regulate hypertrophy in cultured rat cardiac myocytes. *J Formos Med Assoc* **112**, 635-643.

Wang, H., Jing, R., Trexler, C., Li, Y., Tang, H., Pan, Z., Zhu, S., Zhao, B., Fang, X., Liu, J., et al. (2019). Deletion of IP(3)R1 by Pdgfrb-Cre in mice results in intestinal pseudo-obstruction and lethality. *J Gastroenterol* **54**, 407-418.

Wang, S., Zaitoun, I. S., Johnson, R. P., Jamali, N., Gurel, Z., Wintheiser, C. M., Strasser, A., Lindner, V., Sheibani, N. and Sorenson, C. M. (2017). Bim expression in endothelial cells and pericytes is essential for regression of the fetal ocular vasculature. *PLoS One* **12**, e0178198.

Wettschureck, N., Lee, E., Libutti, S. K., Offermanns, S., Robey, P. G. and Spiegel, A. M. (2007). Parathyroid-specific double knockout of Gq and G11 alpha-subunits leads to a phenotype resembling germline knockout of the extracellular Ca2+ -sensing receptor. *Mol Endocrinol* **21**, 274-280.

Wettschureck, N., Moers, A., Hamalainen, T., Lemberger, T., Schutz, G. and Offermanns, S. (2004). Heterotrimeric G proteins of the Gq/11 family are crucial for the induction of maternal behavior in mice. *Mol Cell Biol* **24**, 8048-8054.

Development • Accepted manuscript

Wettschureck, N., Moers, A., Wallenwein, B., Parlow, A. F., Maser-Gluth, C. and Offermanns, S. (2005). Loss of Gq/11 family G proteins in the nervous system causes pituitary somatotroph hypoplasia and dwarfism in mice. *Mol Cell Biol* **25**, 1942-1948.

Wettschureck, N., Rutten, H., Zywietz, A., Gehring, D., Wilkie, T. M., Chen, J., Chien, K. R. and Offermanns, S. (2001). Absence of pressure overload induced myocardial hypertrophy after conditional inactivation of Galphaq/Galpha11 in cardiomyocytes. *Nat Med* **7**, 1236-1240.

Wettschureck, N., van der Stelt, M., Tsubokawa, H., Krestel, H., Moers, A., Petrosino, S., Schutz, G., Di Marzo, V. and Offermanns, S. (2006). Forebrain-specific inactivation of Gq/G11 family G proteins results in age-dependent epilepsy and impaired endocannabinoid formation. *Mol Cell Biol* **26**, 5888-5894.

www.ipfcellatlas.com (2020). IPF Cell Atlas Researchers. www.ipfcellatlas.com. Kaminski/Rosas dataset. (ed N. N).

www.lungmap.net LungMAP consortium. www.lungmap.net. pp. The LungMAP consortium and the LungMAP Data Coordinating Center (1U01HL122638) are funded by the National Heart, Lung, and Blood Institute (NHLBI).

Xu, M. Y., Porte, J., Knox, A. J., Weinreb, P. H., Maher, T. M., Violette, S. M., McAnulty, R. J., Sheppard, D. and Jenkins, G. (2009). Lysophosphatidic acid induces alphavbeta6 integrin-mediated TGF-beta activation via the LPA2 receptor and the small G protein G alpha(q). *Am J Pathol* **174**, 1264-1279.

Zaitoun, I. S., Wintheiser, C. M., Jamali, N., Wang, S., Suscha, A., Darjatmoko, S. R., Schleck, K., Hanna, B. A., Lindner, V., Sheibani, N., et al. (2019). Bcl-2 Expression in Pericytes and Astrocytes Impacts Vascular Development and Homeostasis. *Sci Rep* **9**, 9700.

Zhang, J., Hou, Z., Wang, X., Jiang, H., Neng, L., Zhang, Y., Yu, Q., Burwood, G., Song, J., Auer, M., et al. (2021). VEGFA165 gene therapy ameliorates blood-labyrinth barrier breakdown and hearing loss. *JCI Insight* **6**.

Zou, X., Ramachandran, P., Kendall, T. J., Pellicoro, A., Dora, E., Aucott, R. L., Manwani, K., Man, T. Y., Chapman, K. E., Henderson, N. C., et al. (2018). 11Beta-hydroxysteroid dehydrogenase-1 deficiency or inhibition enhances hepatic myofibroblast activation in murine liver fibrosis. *Hepatology* **67**, 2167-2181.

Zywietz, A., Gohla, A., Schmelz, M., Schultz, G. and Offermanns, S. (2001). Pleiotropic effects of Pasteurella multocida toxin are mediated by Gq-dependent and -independent mechanisms. involvement of Gq but not G11. *J Biol Chem* **276**, 3840-3845.

Development • Accepted manuscript

Figures

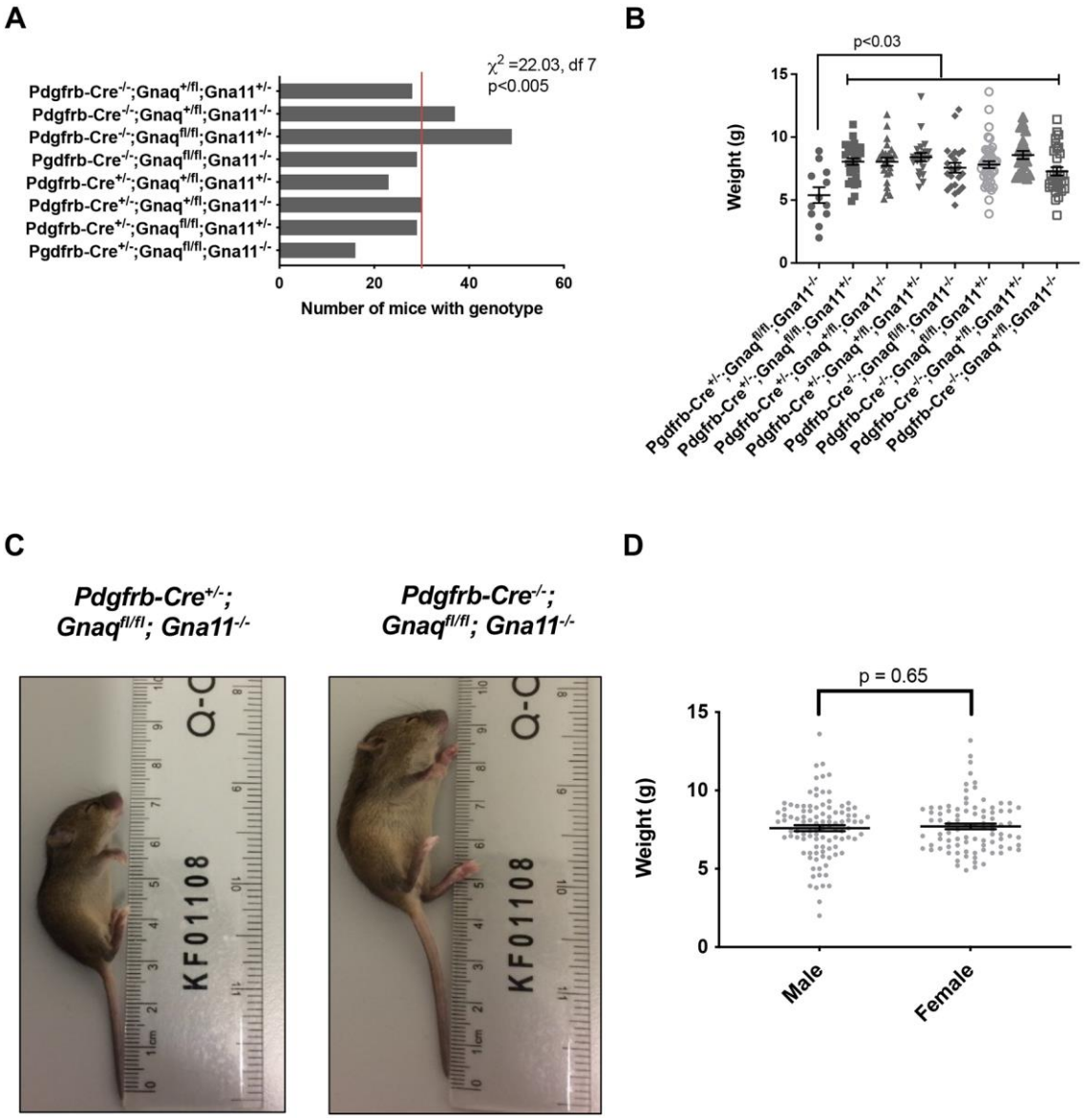

Fig. 1: *Pdgfrb-Cre*$^{+/-}$*;Gnaq*$^{fl/fl}$*;Gna11*$^{-/-}$ mice are growth restricted

A) Genotype frequencies from *Pdgfrb-Cre*$^{+/-}$ x *Gnaq*$^{fl/fl}$*;Gna11*$^{-/-}$ breeding. Red line indicates the expected frequency for each genotype (n=30, 12.5%). Total number of mice born = 241, 24 litters, mean litter size 7.4. Chi-squared value (χ^2) = 22.03, degrees of freedom =7, p<0.005.

B) Body weights of P14 pups by genotype. Mean ± SEM, one way ANOVA with Tukey's multiple comparisons test, n = 12 *Pdgfrb-Cre*$^{+/-}$ x *Gnaq*$^{fl/fl}$*;Gna11*$^{-/-}$ mice, n= 21-43 for other genotypes.

Development • Accepted manuscript

C) Photograph of a P14 pup with the *Pdgfrb-Cre*$^{+/-}$*; Gnaq*$^{fl/fl}$*; Gna11*$^{-/-}$ genotype (left), and a *Pdgfrb-Cre*$^{-/-}$*; Gnaq*$^{fl/fl}$*;Gna11*$^{-/-}$ control littermate (right).

D) Body weights of all pups from *Pdgfrb-Cre*$^{+/-}$ *x Gnaq*$^{fl/fl}$*;Gna11*$^{-/-}$ crosses by sex at P14. Mean ± SEM, unpaired two-tailed Student's t-test, 88 female and 102 male mice.

Df= degrees of freedon; SEM= standard error of the mean; P14= postnatal day 14

Development • Accepted manuscript

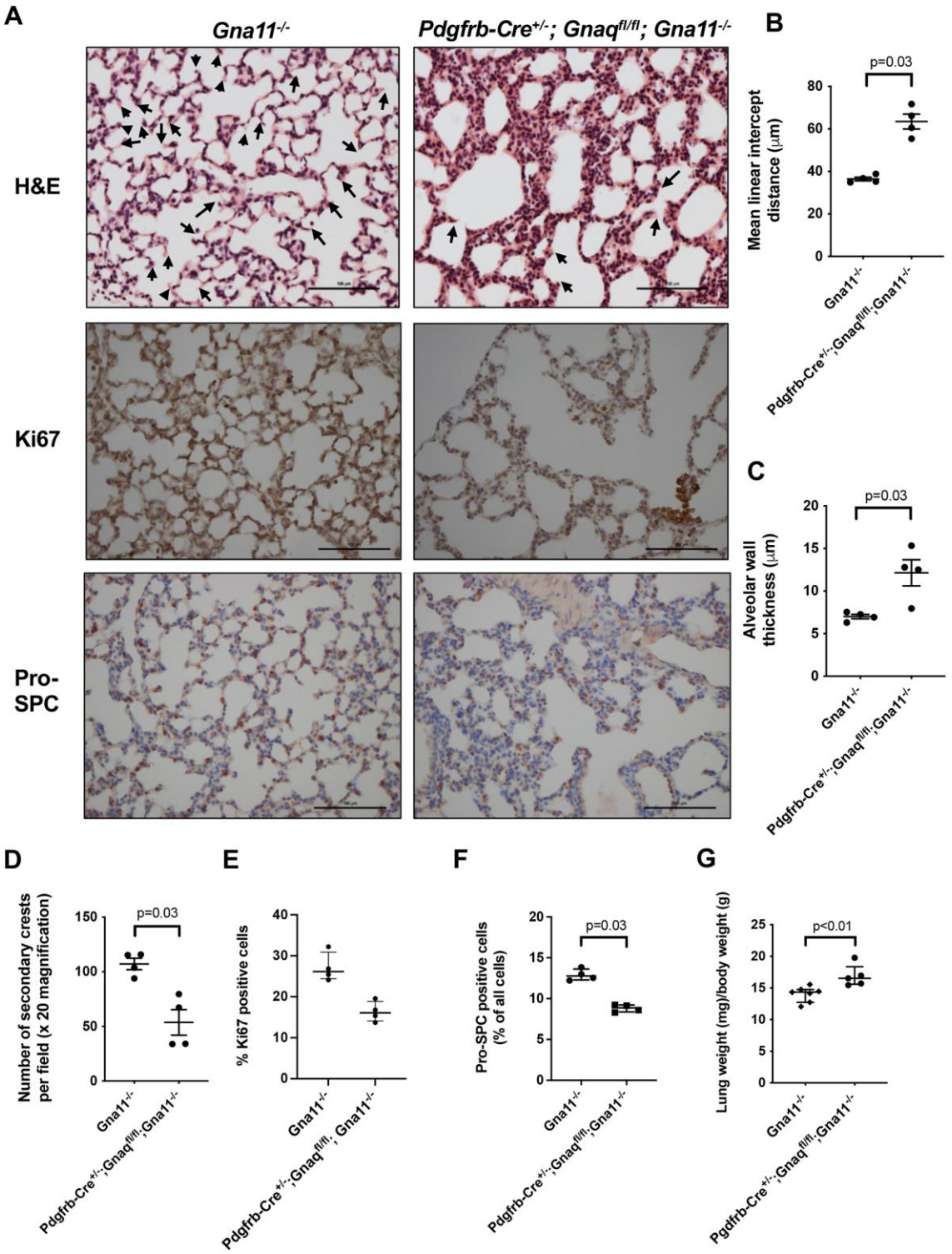

Fig. 2. *Pdgfrb-Cre*$^{+/-}$*;Gnaq*$^{fl/fl}$*;Gna11*$^{-/-}$ mice have abnormal lung appearances characteristic of disturbed alveologenesis

A) Haematoxylin and eosin (H&E) (top), Ki67 immunohistochemistry (middle), and pro-SPC immunohistochemistry (bottom) staining of lungs from P14 *Gna11*$^{-/-}$ (left) and *Pdgfrb-Cre*$^{+/-}$*;Gnaq*$^{fl/fl}$*;Gna11*$^{-/-}$ mice (right). Arrows on H&E images indicate

Development • Accepted manuscript

secondary crests. Images representative of 4 mice per group. Scale bars show 100µm.

B) Mean linear intercept analysis of airspace size in P14 *Gna11*$^{-/-}$ and *Pdgfrb-Cre*$^{+/}$;*Gnaq*$^{fl/fl}$;*Gna11*$^{-/-}$ mice. Median ± interquartile range, n=4 mice per group, two-tailed Mann Whitney test.

C) Alveolar wall thickness in P14 *Gna11*$^{-/-}$ and *Pdgfrb-Cre*$^{+/-}$;*Gnaq*$^{fl/fl}$;*Gna11*$^{-/-}$ mice. Median ± interquartile range, n=4 mice per group, two-tailed Mann Whitney test.

D) Quantification of the number of secondary crests per 20 x field in P14 *Gna11*$^{-/-}$ and *Pdgfrb-Cre*$^{+/-}$;*Gnaq*$^{fl/fl}$;*Gna11*$^{-/-}$ mice. Median ± interquartile range, n=4 mice per group, two-tailed Mann Whitney test.

E) Quantification of Ki67 immunohistochemistry in P14 *Gna11*$^{-/-}$ and *Pdgfrb-Cre*$^{+/-}$;*Gnaq*$^{fl/fl}$;*Gna11*$^{-/-}$ mice. Shown as the percentage of Ki67 positive nuclei per 40x magnification field. Median ± interquartile range, n=4 mice per group, two-tailed Mann Whitney test.

F) Quantification of Pro-SPC immunohistochemistry in P14 *Gna11*$^{-/-}$ and *Pdgfrb-Cre*$^{+/-}$;*Gnaq*$^{fl/fl}$;*Gna11*$^{-/-}$ mice. Shown as the percentage of pro-SPC positive cells per 40x magnification field. Median ± interquartile range, n=4 mice per group, two-tailed Mann Whitney test.

G) Relative lung to total body weights in P14 *Gna11*$^{-/-}$ and *Pdgfrb-Cre*$^{+/-}$;*Gnaq*$^{fl/fl}$;*Gna11*$^{-/-}$ mice. Median ± interquartile range, n=5 *Pdgfrb-Cre*$^{+/-}$;*Gnaq*$^{fl/fl}$;*Gna11*$^{-/-}$ mice, n=6 *Gna11*$^{-/-}$ controls, two-tailed Mann Whitney test.

H&E= haematoxylin and eosin; Pro-SPC= pro-surfactant protein C; P14= postnatal day 14; *Gna11*$^{-/-}$= *Pdgfrb-Cre*$^{-/-}$;*Gnaq*$^{fl/fl}$;*Gna11*$^{-/-}$ littermate controls

Development • Accepted manuscript

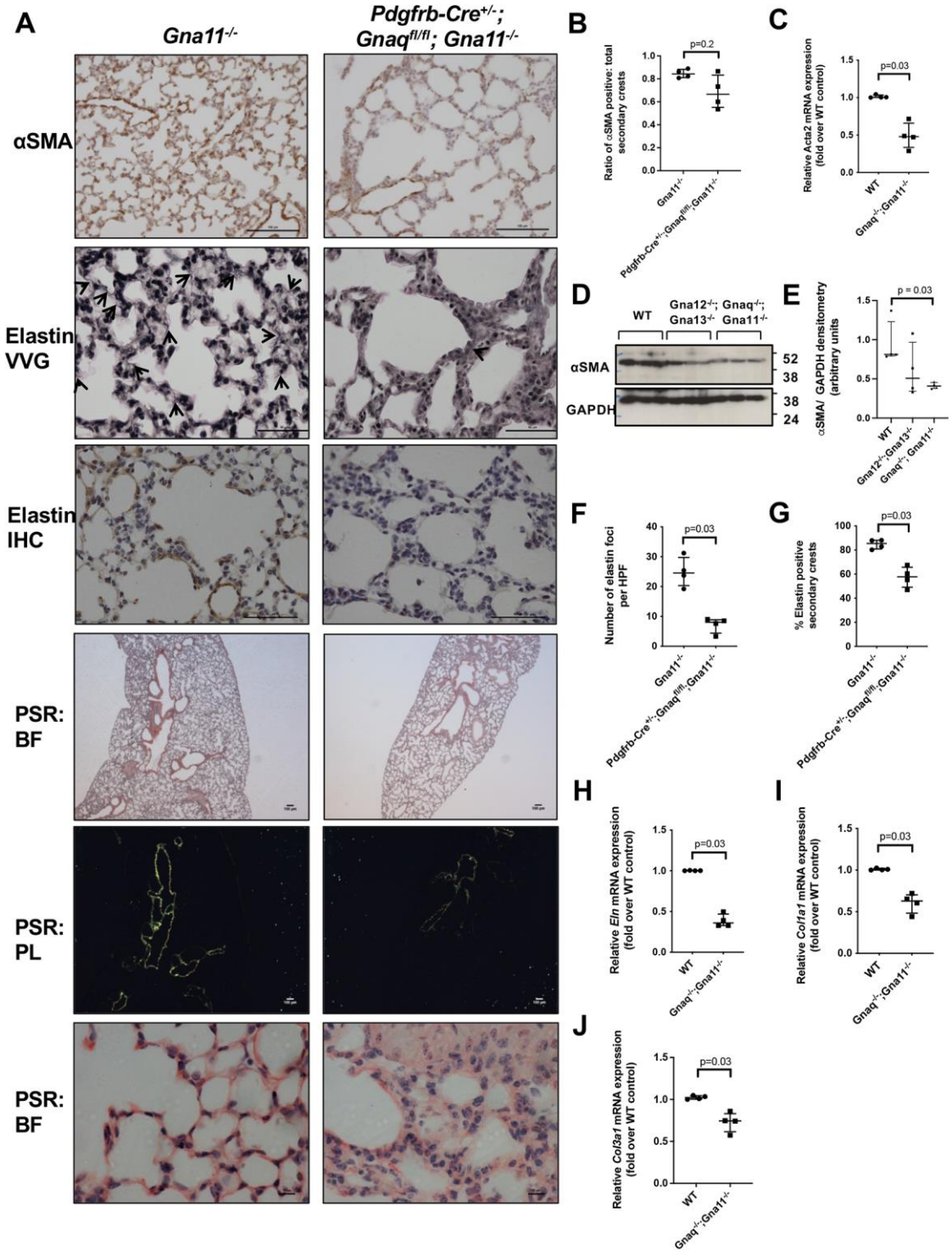

Fig. 3. *Pdgfrb-Cre*$^{+/-}$*;Gnaq*$^{fl/fl}$*;Gna11*$^{-/-}$ mice have reduced lung myofibroblast differentiation and function

A) αSMA immunohistochemistry (row 1), elastin Verhoeff van Gieson (VVG) stain (row 2), elastin immunohistochemistry (row 3), and picrosirius red (PSR) staining (row 4-6) from P14 *Gna11*$^{-/-}$ (left) and *Pdgfrb-Cre*$^{+/-}$*;Gnaq*$^{fl/fl}$*;Gna11*$^{-/-}$ (right) mice. Arrows on

Development • Accepted manuscript

elastin images shown elastin foci. Picrosirius red images shown are bright field (BF, row 4), polarised light (row 5), and bright field at high magnification (row 5). Representative images from 4 mice per genotype. Scale bars show 100μm (αSMA, PSR), 50μm (elastin VVG and IHC), and 10μm (picrosirius red high magnification).

B) Quantification of the proportion of secondary crests that stained positively for αSMA in P14 *Gna11*$^{-/-}$ and *Pdgfrb-Cre*$^{+/-}$;*Gnaq*$^{fl/fl}$;*Gna11*$^{-/-}$ lungs. Median ± interquartile range, n=4 mice per group, two-tailed Mann Whitney test.

C) *Acta2* mRNA expression in WT and *Gnaq*$^{-/-}$;*Gna11*$^{-/-}$ MEFs. Median ± interquartile range, n=4 per group, two-tailed Mann Whitney test.

D) Representative western blot showing αSMA expression in wild-type (WT), *Gna12*$^{-/-}$;*Gna13*$^{-/-}$, and *Gnaq*$^{-/-}$;*Gna11*$^{-/-}$ MEFs.

E) Densitometry of western blots of αSMA expression in wild-type (WT), *Gna12*$^{-/-}$;*Gna13*$^{-/-}$, and *Gnaq*$^{-/-}$;*Gna11*$^{-/-}$ MEFs. Median ± interquartile range, n=4, two-tailed Mann Whitney test.

F) The number of elastin foci per high powered field (HPF) (40x magnification) in P14 *Gna11*$^{-/-}$ and *Pdgfrb-Cre*$^{+/-}$;*Gnaq*$^{fl/fl}$;*Gna11*$^{-/-}$ lungs. Median ± interquartile range, n=4 mice per group, two-tailed Mann Whitney test.

G) The proportion of secondary crests that stained positively for elastin in each high powered field (40 x magnification) in P14 *Gna11*$^{-/-}$ and *Pdgfrb-Cre*$^{+/-}$;*Gnaq*$^{fl/fl}$;*Gna11*$^{-/-}$ lungs. Median ± interquartile range, n=4 mice per group, two-tailed Mann Whitney test.

H) *Eln* mRNA expression in wild-type (WT) and *Gnaq*$^{-/-}$;*Gna11*$^{-/-}$ MEFs. Median ± interquartile range, n=4, two-tailed Mann Whitney test.

I) *Col1a1* mRNA expression in wild-type (WT) and *Gnaq*$^{-/-}$;*Gna11*$^{-/-}$ MEFs. Median ± interquartile range, n=4, two-tailed Mann Whitney test.

J) *Col3a1* mRNA expression in wild-type (WT) and *Gnaq*$^{-/-}$;*Gna11*$^{-/-}$ MEFs. Median ± interquartile range, n=4, two-tailed Mann Whitney test.

αSMA= α smooth muscle actin; P14= postnatal day 14; VVG= Verhoeff van Gieson; IHC= immunohistochemistry; PSR= picrosirius red; BF= brightfield; PL= polarised light; *Gna11*$^{-/-}$= *Pdgfrb-Cre*$^{-/-}$;*Gnaq*$^{fl/fl}$;*Gna11*$^{-/-}$ littermate controls; WT= wild-type; MEFs= murine embryonic fibroblasts; HPF= high powered field

Development • Accepted manuscript

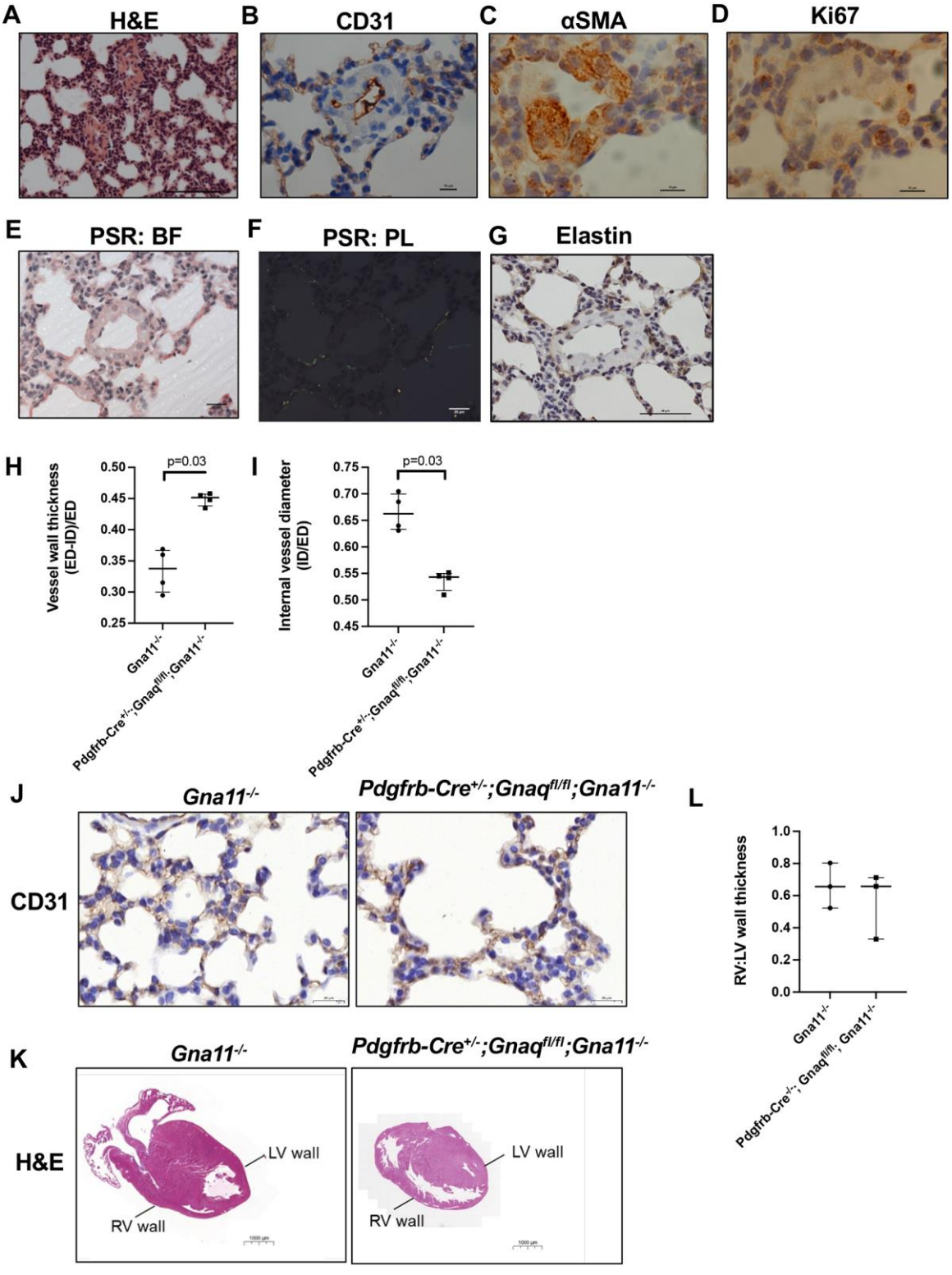

Fig. 4. The lungs of *Pdgfrb-Cre$^{+/-}$;Gnaq$^{fl/fl}$;Gna11$^{-/-}$* mice contain abnormal peripheral pulmonary vessels.

A-G) Lung sections from P14 *Pdgfrb-Cre$^{+/-}$;Gnaq$^{fl/fl}$;Gna11$^{-/-}$* mice were stained using various techniques.

Development • Accepted manuscript

A) Haematoxylin and eosin (H&E) stain. Scale bar shows 100µm.

B) CD31 immunohistochemistry. Scale bar shows 10µm.

C) αSMA immunohistochemistry. Scale bar shows 10µm.

D) Ki67 immunohistochemistry. Scale bar shows 10µm.

E) Picrosirius red stain (PSR). Same image shown using bright field (BF, E) and polarised light (PL, F) illumination). Scale bar shows 20µm.

G) Elastin immunohistochemistry. Scale bar shows 50µm.

H) Quantification of peripheral vessel wall thickness in P14 *Gna11*$^{-/-}$ and *Pdgfrb-Cre*$^{+/-}$*;Gnaq*$^{fl/fl}$*;Gna11*$^{-/-}$ lungs. Vessel wall thickness calculated as (external diameter (ED)– internal diameter)/ external diameter. Median ± interquartile range, n=4 mice per group, two-tailed Mann Whitney test.

I) Quantification of vessel lumen diameter in P14 *Gna11*$^{-/-}$ and *Pdgfrb-Cre*$^{+/-}$*;Gnaq*$^{fl/fl}$*;Gna11*$^{-/-}$ lungs. Vessel lumen diameter calculated as internal diameter (ID)/ external diameter (ED). Median ± interquartile range, n=4 mice per group, two-tailed Mann Whitney test.

J) CD31 immunohistochemistry from P14 *Gna11*$^{-/-}$ (left) and *Pdgfrb-Cre*$^{+/-}$*;Gnaq*$^{fl/fl}$*;Gna11*$^{-/-}$ (right) mice. Representative images from 4 mice per genotype. Scale bars show 20µm.

K) Haematoxylin and eosin stain of representative hearts from P14 *Gna11*$^{-/-}$ (left) and *Pdgfrb-Cre*$^{+/-}$*;Gnaq*$^{fl/fl}$*;Gna11*$^{-/-}$ (right) mice. Scale bars show 1000µm.

L) Right: left cardiac ventricular wall thickness ratios in P14 *Gna11*$^{-/-}$ (left) and *Pdgfrb-Cre*$^{+/-}$*;Gnaq*$^{fl/fl}$*;Gna11*$^{-/-}$ (right) mice. Median ± interquartile range, n=3 mice per group.

H&E= haematoxylin and eosin; αSMA= α-smooth muscle actin; P14= postnatal day 14; PSR= picrosirius red; BF= brightfield; PL= polarised light; *Gna11*$^{-/-}$= *Pdgfrb-Cre*$^{-/-}$*;Gnaq*$^{fl/fl}$*;Gna11*$^{-/-}$ littermate controls; ED= external diameter; ID= internal diameter; RV= right ventricle; LV= left ventricle;

Development • Accepted manuscript

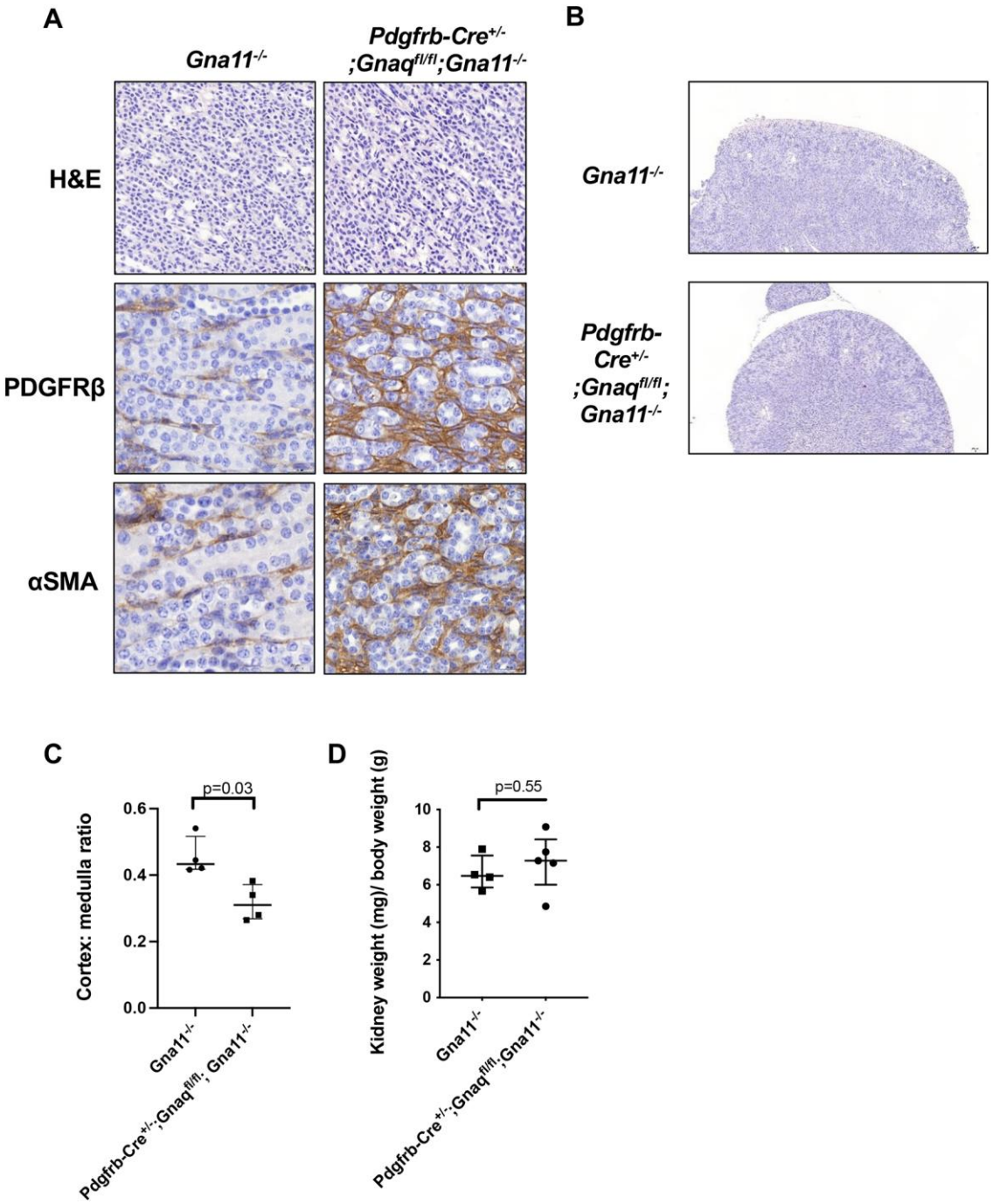

Fig. 5. *Pdgfrb-Cre$^{+/-}$;Gnaq$^{fl/fl}$;Gna11$^{-/-}$* mice have kidney abnormalities

A) Haematoxylin and eosin (H&E), PDGFRβ immunohistochemistry, and αSMA immunohistochemistry of renal medulla, images of P14 *Gna11$^{-/-}$* and *Pdgfrb-Cre$^{+/-}$;Gnaq$^{fl/fl}$;Gna11$^{-/-}$* mouse kidneys. Representative images from 4 mice per genotype. Scale bars show 20µm.

B) Low magnification images of haematoxylin and eosin staining of P14 *Gna11$^{-/-}$* (top) and *Pdgfrb-Cre$^{+/-}$;Gnaq$^{fl/fl}$;Gna11$^{-/-}$* (bottom) mice. Scale bars show 200µm.

Development • Accepted manuscript

C) Cortex: medulla ratios of P14 *Gna11*$^{-/-}$ and *Pdgfrb-Cre*$^{+/-}$;*Gnaq*$^{fl/fl}$;*Gna11*$^{-/}$ mice. Median ± interquartile range, n=4 mice per group, two-tailed Mann Whitney test.

D) Relative kidney: total body weight in P14 *Gna11*$^{-/-}$ and *Pdgfrb-Cre*$^{+/-}$;*Gnaq*$^{fl/fl}$;*Gna11*$^{-/-}$ mice.

H&E= haematoxylin and eosin; PDGFRβ= platelet derived growth factor receptor β; αSMA= α-smooth muscle actin; *Gna11*$^{-/-}$= *Pdgfrb-Cre*$^{-/-}$;*Gnaq*$^{fl/fl}$;*Gna11*$^{-/-}$ littermate controls; P14= postnatal day 14

Development • Accepted manuscript

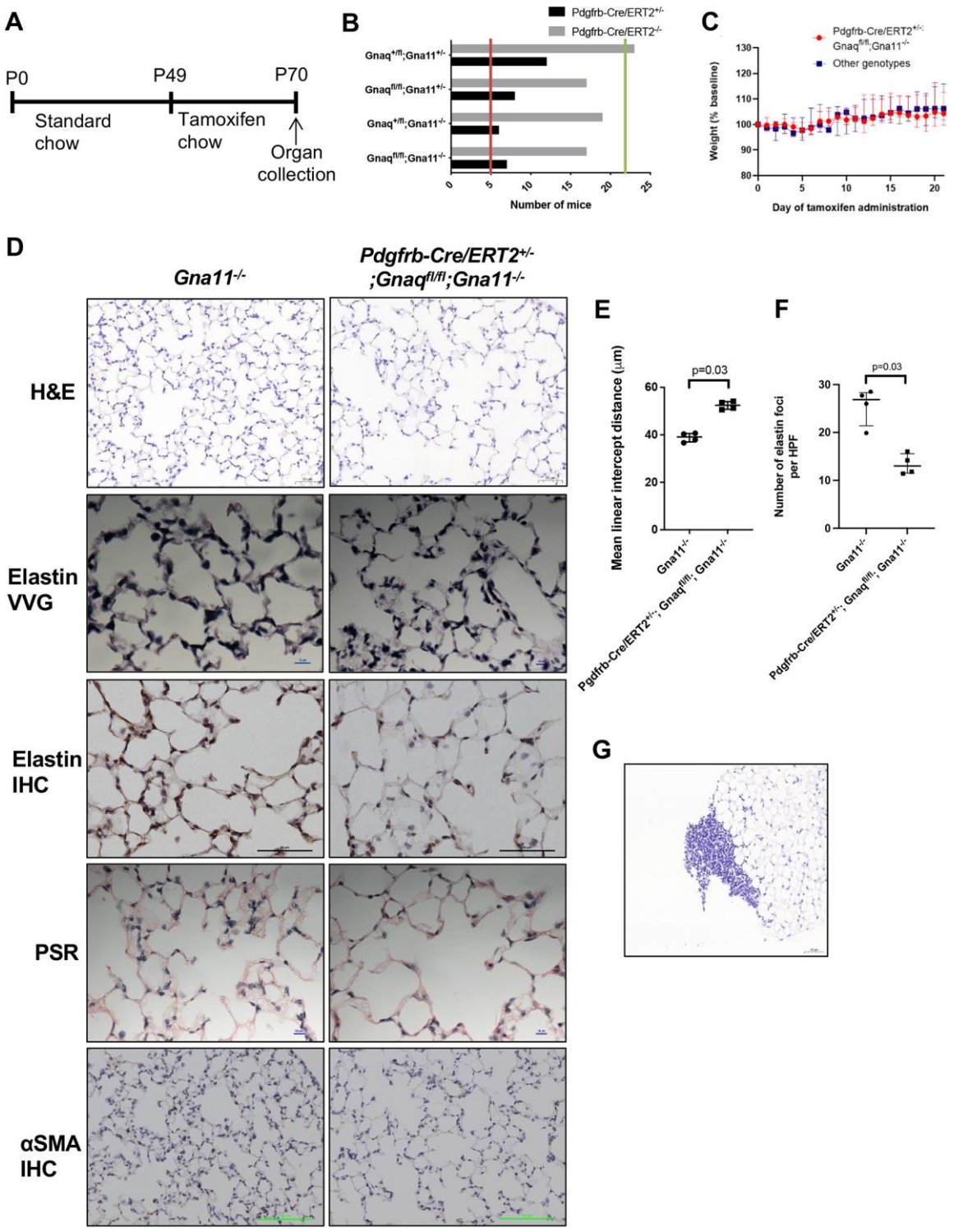

Fig. 6. Mice with mesenchymal $G_{\alpha q/11}$ deletion in adulthood develop emphysema

A) Protocol for tamoxifen administration in *Pdgfrb-Cre/ERT2*$^{+/-}$ x *Gnaq*$^{fl/fl}$*;Gna11*$^{-/-}$ mouse colony.

B) Genotype frequencies from *Pdgfrb-Cre/ERT2*$^{+/-}$ x *Gnaq*$^{fl/fl}$*;Gna11*$^{-/-}$ breeding. Red line indicates the expected frequency of Pdgfrb-Cre/ERT2$^{+/-}$ genotypes (5%, n =5), and

Development • Accepted manuscript

green line indicates expected frequency of Pdgfrb-Cre/ERT2$^{-/-}$ genotypes (20%, n=. 22, total n=109, 20 litters, mean litter size 5.5).

C) Weights of *Pdgfrb-Cre/ERT2*$^{+/-}$*;Gnaq*$^{fl/fl}$*;Gna11*$^{-/}$ mice (red) and littermates of all other genotypes (blue) during 21 days of tamoxifen administration.

D) Histology of lungs from *Gna11*$^{-/-}$ control (left) and *Pdgfrb-Cre/ERT2*$^{+/-}$*;Gnaq*$^{fl/fl}$*;Gna11*$^{-/-}$ (right) mice. Haematoxylin and eosin (row 1), elastin Verhoeff van Gieson (VVG, row 2), elastin immunohistochemistry (row 3), picrosirius red (PSR, row 4), and αSMA immunohistochemistry (row 5). Representative images from 4 mice per genotype. Scale bars show 50μm (H&E), 10μm (elastin VVG, PSR), 50μm (elastin IHC), and 100μm (αSMA IHC).

E) Mean linear intercept distance in *Gna11*$^{-/-}$ and *Pdgfrb-Cre/ERT2*$^{+/-}$*;Gnaq*$^{fl/fl}$*;Gna11*$^{-/-}$ mouse lungs. Median ± interquartile range, n=4 mice per group, two-tailed Mann Whitney test.

F) Quantification of elastin foci in *Gna11*$^{-/-}$ and *Pdgfrb-Cre/ERT2*$^{+/-}$*;Gnaq*$^{fl/fl}$*;Gna11*$^{-/-}$ mouse lungs. Median ± interquartile range, n=4 mice per group, two-tailed Mann Whitney test.

G) Representative image of mononuclear cell infiltrates seen in *Pdgfrb-Cre/ERT2*$^{+/-}$ *;Gnaq*$^{fl/fl}$*;Gna11*$^{-/-}$ mouse lungs.

P0= postnatal day 0; P49= postnatal day 49; P70= postnatal day 70; *Gna11*$^{-/-}$= *Pdgfrb-Cre/ERT2*$^{-/-}$*;Gnaq*$^{fl/fl}$*;Gna11*$^{-/-}$ controls; H&E= haematoxylin and eosin; VVG= Verhoeff van Gieson; IHC= immunohistochemistry; PSR= picrosirius red; αSMA= α-smooth muscle actin

Development • Accepted manuscript

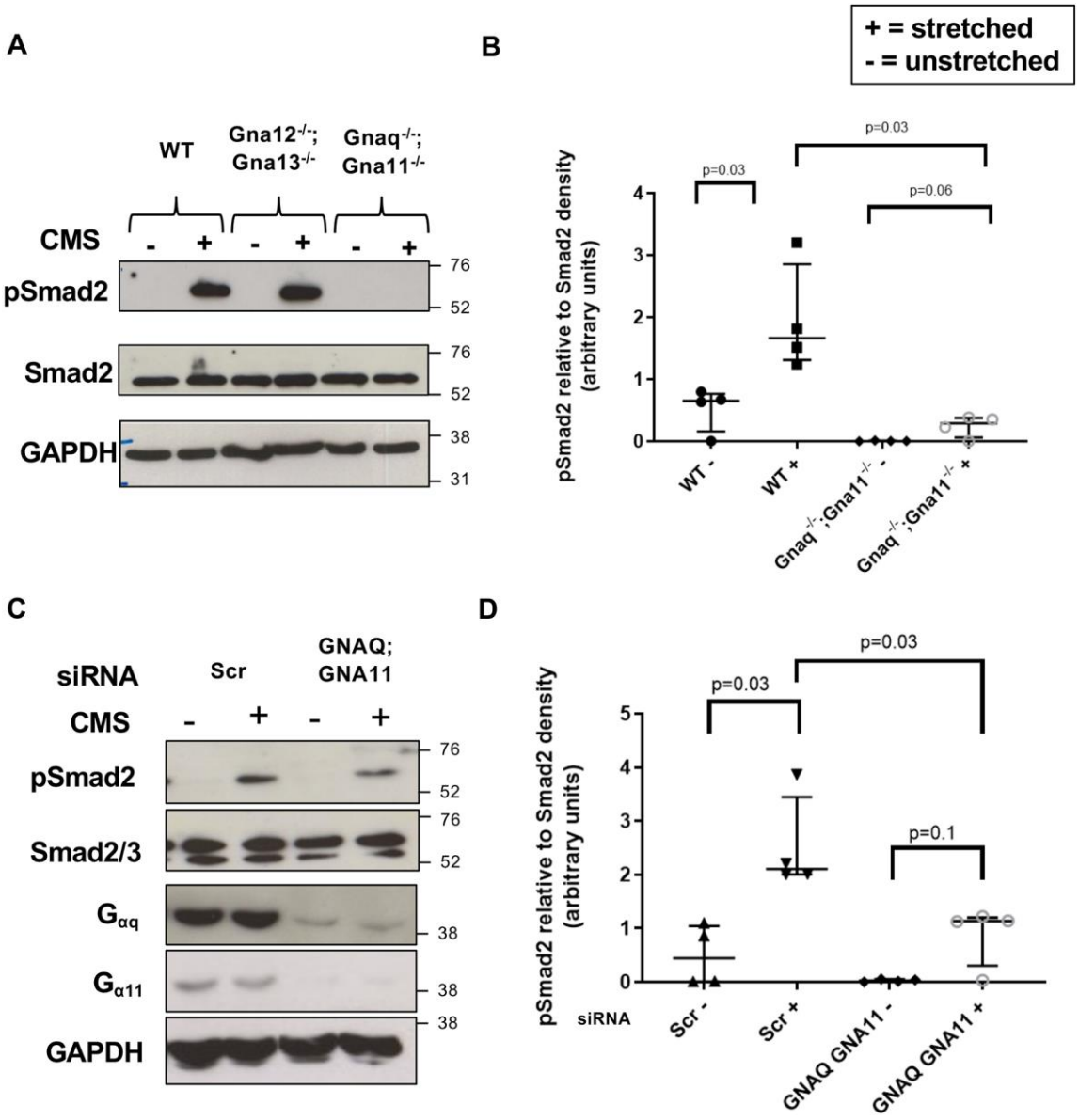

Fig. 7. $G_{\alpha q/11}$ mediates stretch-induced TGFβ signalling in murine and human fibroblasts

A) Representative western blot showing pSmad2 expression in wild-type (WT), *Gna12*$^{-/-}$*;Gna13*$^{-/-}$, and *Gnaq*$^{-/-}$*Gna11*$^{-/-}$ MEFs subject to cyclical mechanical stretch (CMS) (15% elongation, 1Hz, 48 hours).

B) Densitometry of western blots from stretched MEFs shown as pSmad2 relative to Smad2 expression from 4 independent experiments. Median ± interquartile range, n=4, two-tailed Mann Whitney Test.

C) Representative western blot showing pSmad2 expression in HLFs treated with non-targeting (Scr) or *GNAQ* and *GNA11* siRNA then subject to cyclical mechanical stretch (15% elongation, 0.3Hz, 24 hours).

Development • Accepted manuscript

D) Densitometry of western blots from stretched HLFs shown as pSmad2 relative to Smad2 expression from 4 independent experiments. Median ± interquartile range, n=4, two-tailed Mann Whitney Test.

+= stretched; -= unstretched; CMS= cyclical mechanical stretch; WT= wild-type; siRNA= small interfering RNA; Scr= scrambled (control siRNA)

Development • Accepted manuscript

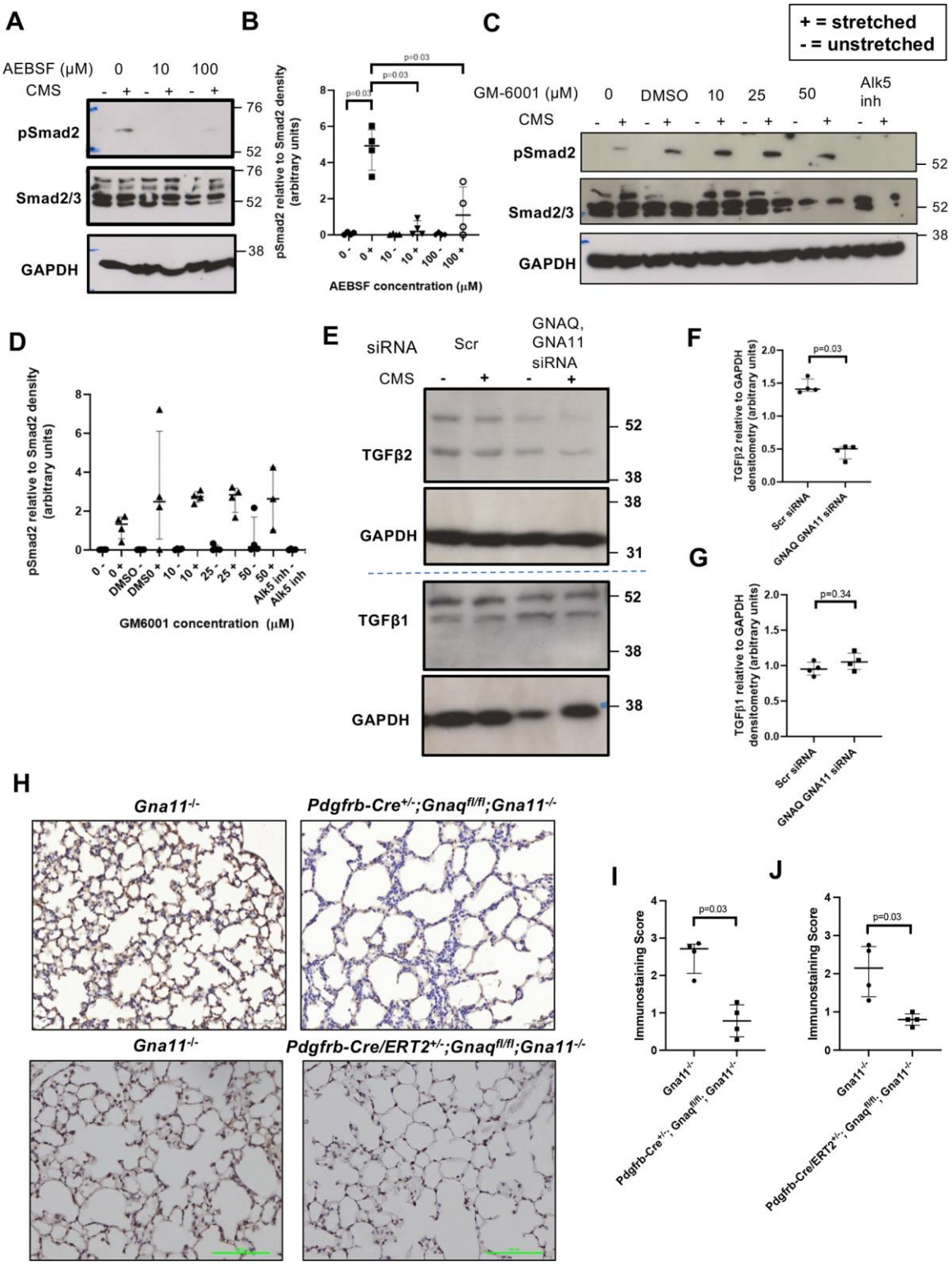

Development • Accepted manuscript

Fig. 8. $G_{\alpha q/11}$ signalling induces the production of TGFβ2 which is then available for stretch-induced serine protease-mediated activation

A) Representative pSmad2 western blot of human lung fibroblasts treated with the serine protease inhibitor AEBSF then subject to cyclical mechanical stretch (CMS) (15% elongation, 0.3Hz, 48 hours).

B) Relative pSmad2 to Smad2 densitometry of human lung fibroblasts treated with AEBSF then subject to cyclical mechanical stretch. Median ± interquartile range, n=4, two-tailed Mann Whitney test.

C) Representative pSmad2 western blot of human lung fibroblasts treated with the matrix metalloproteinase (MMP) inhibitor GM6001 then subject to cyclical mechanical stretch (15% elongation, 0.3Hz, 48 hours).

D) Relative pSmad2 to Smad2 densitometry from human lung fibroblasts treated with GM6001 then subject to cyclical mechanical stretch. Median ± interquartile range, n=4, two-tailed Mann Whitney test.

E) Representative TGFβ2 (top) and TGFβ1 (bottom) western blots of human lung fibroblasts subject to non-targeting (Scr) or *GNAQ* and *GNA11* siRNA and cyclical mechanical stretch (15% elongation, 0.3Hz, 24 hours).

F) Relative TGFβ2 to GAPDH densitometry of human lung fibroblasts with and without siRNA-induced *GNAQ* and *GNA11* knockdown. Median ± interquartile range, n=4, two-tailed Mann Whitney test

G) Relative TGFβ1 to GAPDH densitometry of human lung fibroblasts with and without siRNA-induced *GNAQ* and *GNA11* knockdown. Median ± interquartile range, n=4, two-tailed Mann Whitney test.

H) TGFβ2 immunohistochemistry on P14 *Pdgfrb-Cre*$^{-/-}$;*Gnaq*$^{fl/fl}$;*Gna11*$^{-/-}$ control (left) and *Pdgfrb-Cre*$^{+/-}$;*Gnaq*$^{fl/fl}$;*Gna11*$^{-/-}$ (right) mouse lungs (top row), and tamoxifen-treated P70 *Pdgfrb-Cre/ERT*$^{-/-}$;*Gnaq*$^{fl/fl}$;*Gna11*$^{-/-}$ control (left) and *Pdgfrb-Cre/ERT2*$^{+/-}$;*Gnaq*$^{fl/fl}$;*Gna11*$^{-/-}$ mouse lungs.

I) TGFβ2 immunohistochemistry scores of *Pdgfrb-Cre*$^{-/-}$;*Gnaq*$^{fl/fl}$;*Gna11*$^{-/-}$ control and *Pdgfrb-Cre*$^{+/-}$;*Gnaq*$^{fl/fl}$;*Gna11*$^{-/-}$ mouse lungs. Median ± interquartile range, n=4, two-tailed Mann Whitney test.

J) TGFβ2 immunohistochemistry scores of tamoxifen-treated P70 *Pdgfrb-Cre/ERT2*$^{-/-}$;*Gnaq*$^{fl/fl}$;*Gna11*$^{-/-}$ control and *Pdgfrb-Cre/ERT2*$^{+/-}$;*Gnaq*$^{fl/fl}$;*Gna11*$^{-/-}$ mouse lungs. Median ± interquartile range, n=4, two-tailed Mann Whitney test.

AEBSF= 4-benzenesulfonyl fluoride hydrochloride; += stretched; -= unstretched; Alk5 inh= 50μM Alk5 inhibitor (SB525334); CMS= cyclical mechanical stretch; MMP= matrix metalloproteinase; siRNA= small interfering RNA; Scr= scrambled (control siRNA)

Development • Accepted manuscript

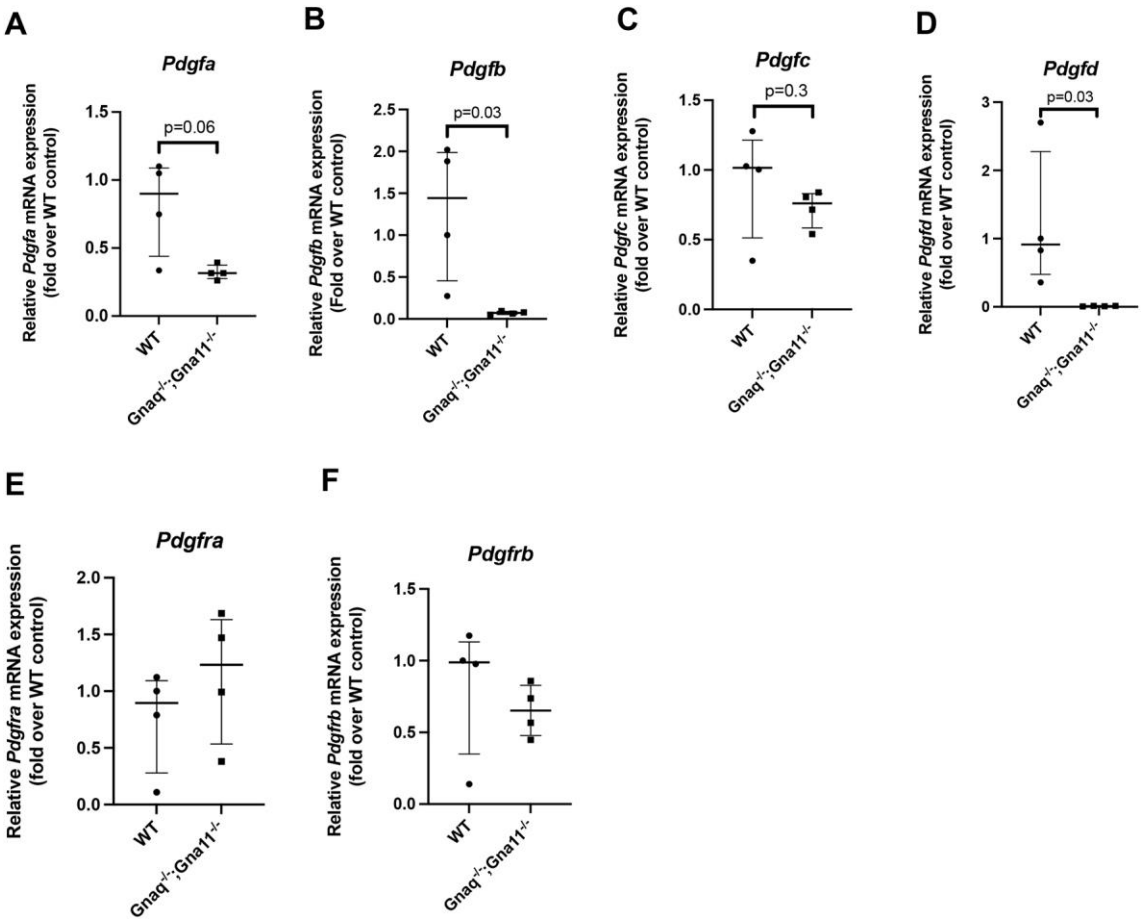

Fig. 9. $G_{\alpha q/11}$ deletion influences expression of some PDGF transcripts in MEFs

Relative mRNA expression of Pdgfa (A), Pdgfb (B), Pdgfc (C), Pdgfd (D), Pgdfra (E), and Pdgfrb (F) in wild-type (WT) and $Gnaq^{-/-}$:$Gna11^{+/-}$ MEFs. Median ± interquartile range, n=4, two-tailed Mann Whitney test.

MEFs= murine embryonic fibroblasts; WT= wild-type

Development • Accepted manuscript

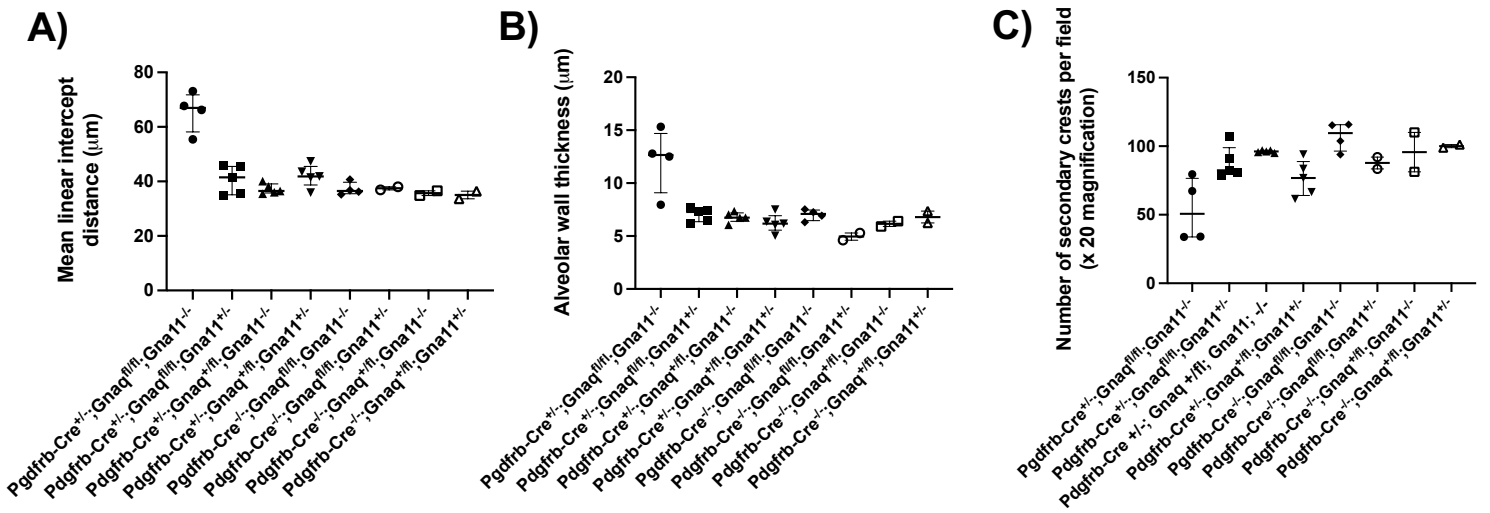

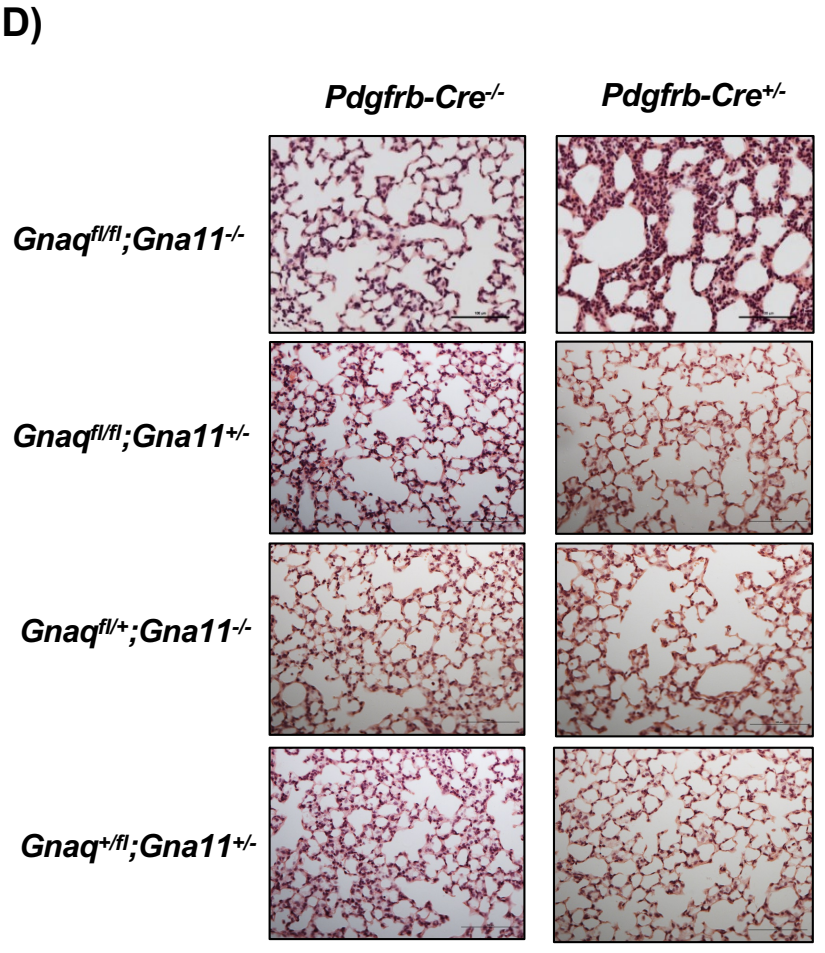

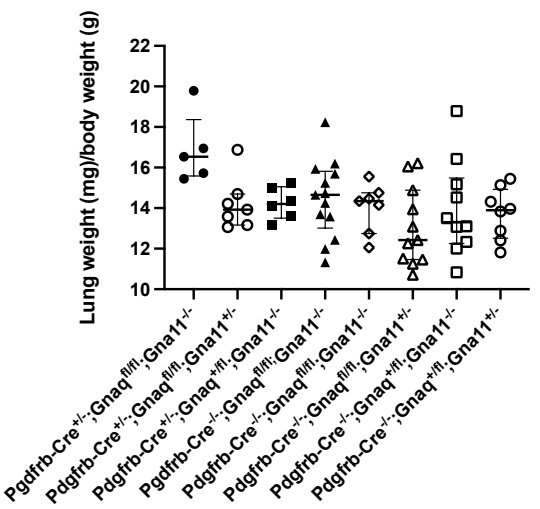

Development • Supplementary information

Fig. S1. Mice with at least one functioning *Gnaq* or *Gna11* allele have normal lung morphology

A) Mean linear intercept measurements from mice of all possible genotypes from the *Pdgfrb-Cre*$^{+/-}$ x *Gnaq*$^{fl/fl}$*;Gna11*$^{-/-}$ breeding programme. Median ± interquartile range, n=2-5 mice per genotype.

B) Alveolar wall thickness measurements from mice of all possible genotypes from the *Pdgfrb-Cre*$^{+/-}$ x *Gnaq*$^{fl/fl}$*;Gna11*$^{-/-}$ breeding programme. Median ± interquartile range, n=2-5 mice per genotype.

C) Quantification of secondary crests from mice of all possible genotypes from the *Pdgfrb-Cre*$^{+/-}$ x *Gnaq*$^{fl/fl}$*;Gna11*$^{-/-}$ breeding programme. Median ± interquartile range, n=2-5 mice per genotype.

D) Representative histology images from mice of all possible genotypes from the *Pdgfrb-Cre*$^{+/-}$ x *Gnaq*$^{fl/fl}$*;Gna11*$^{-/-}$ breeding programme.

E) Relative lung weight (mg) corrected to total body weight (g) of mice of all possible genotypes from the *Pdgfrb-Cre*$^{+/-}$ x *Gnaq*$^{fl/fl}$*;Gna11*$^{-/-}$ breeding programme. Median ± interquartile range, n=5-13 mice per genotype.

Development • Supplementary information

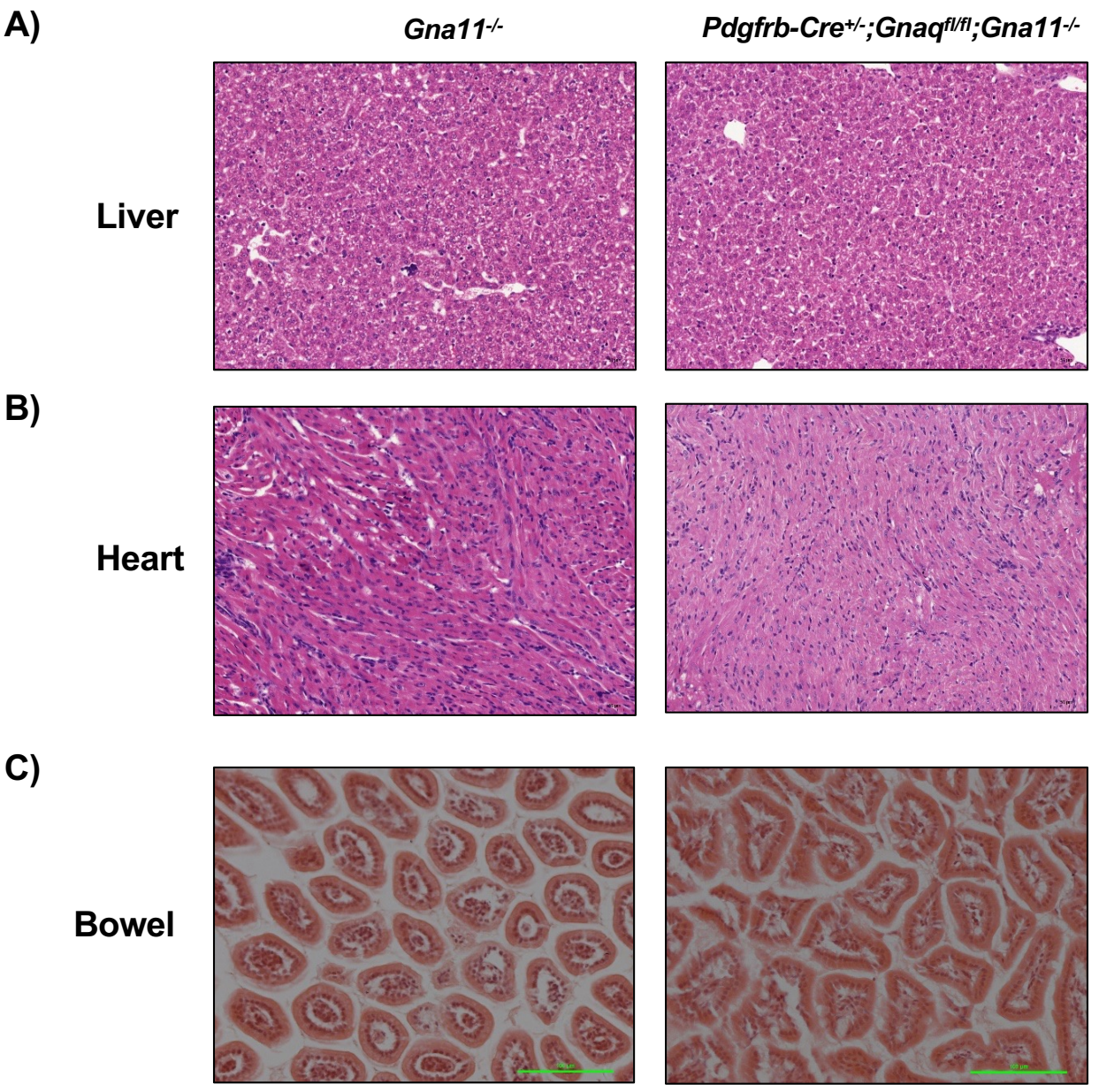

Fig. S2. *Pdgfrb-Cre$^{+/-}$;Gnaq$^{fl/fl}$;Gna11$^{-/-}$* mice have normal liver, heart, and bowel histology.

Representative images of haematoxylin and eosin staining of liver (A), heart (B), and bowel (C) from *Gna11$^{-/-}$* and *Pdgfrb-Cre$^{+/-}$;Gnaq$^{fl/fl}$;Gna11$^{-/-}$* mice.

Gna11$^{-/-}$ = *Pdgfrb-Cre$^{-/-}$;Gnaq$^{fl/fl}$;Gna11$^{-/-}$* littermate controls

Development • Supplementary information

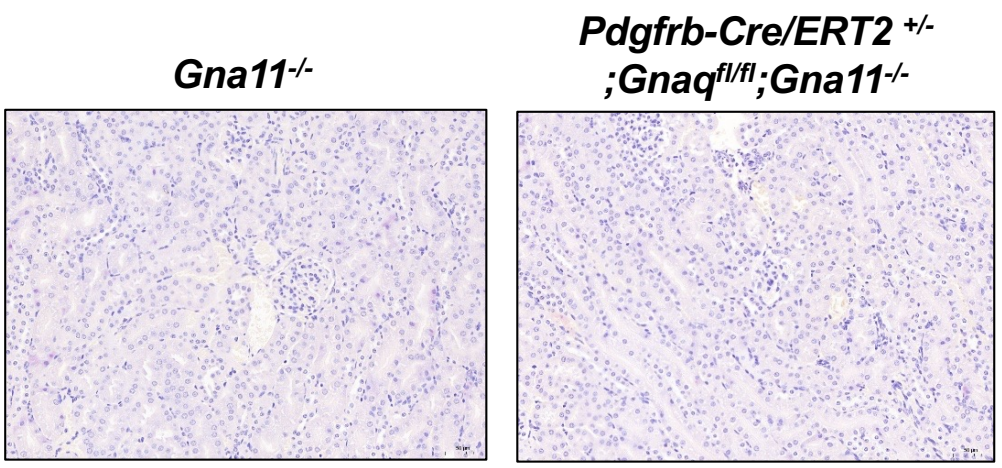

Fig. S3. *Pdgfrb-Cre/ERT2$^{+/-}$;Gnaq$^{fl/fl}$;Gna11$^{-/-}$* mice have normal kidney histology after three weeks of tamoxifen.

Representative images of haematoxylin and eosin staining of kidney from *Gna11$^{-/-}$* and *Pdgfrb-Cre/ERT2$^{+/-}$;Gnaq$^{fl/fl}$;Gna11$^{-/-}$* mice treated with three weeks of tamoxifen.

Gna11$^{-/-}$ = *Pdgfrb-Cre/ERT2$^{-/-}$;Gnaq$^{fl/fl}$;Gna11$^{-/-}$* littermate controls

Development • Supplementary information

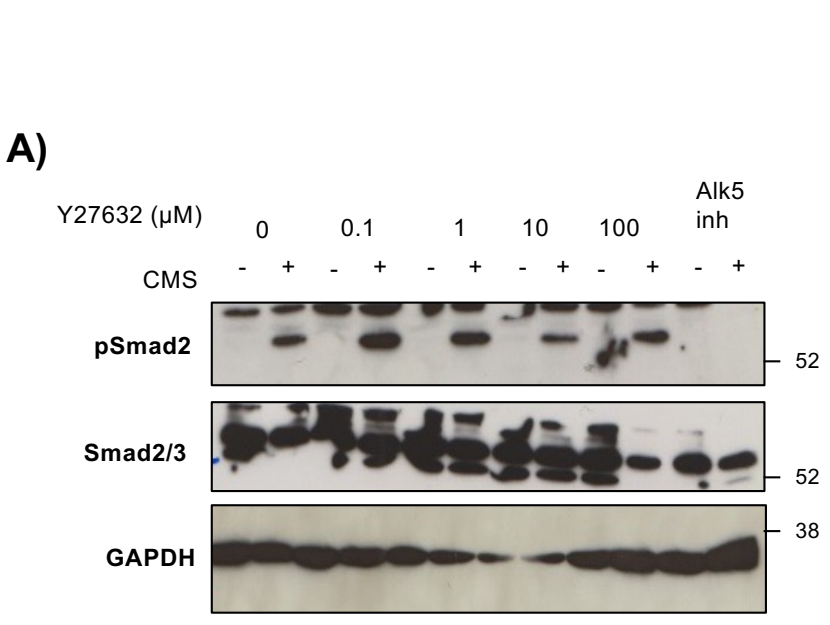
A)
Y27632 (μM)
0
0.1
1
10
100
Alk5 inh
CMS
- + - + - + - + - + - +
pSmad2
Smad2/3
GAPDH
52
52
38

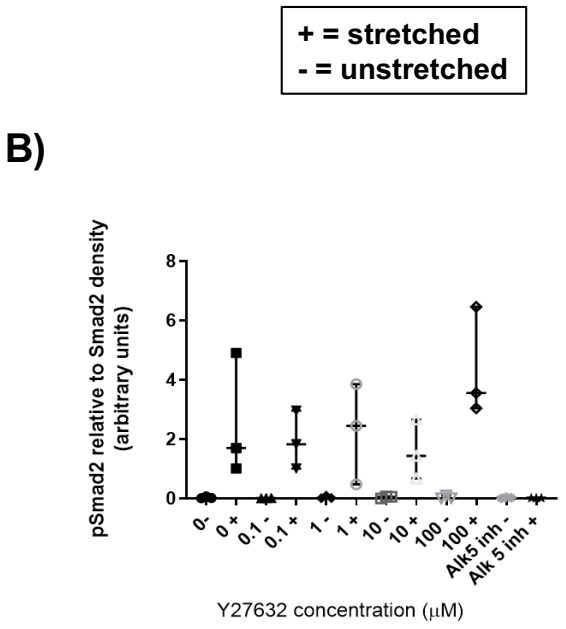
+ = stretched
- = unstretched
B)
pSmad2 relative to Smad2 density (arbitrary units)
0 2 4 6 8
0- 0 + 0.1 - 0.1 + 1 - 1 + 10 - 10 + 100 - 100 + Alk5 inh - Alk 5 inh +
Y27632 concentration (μM)

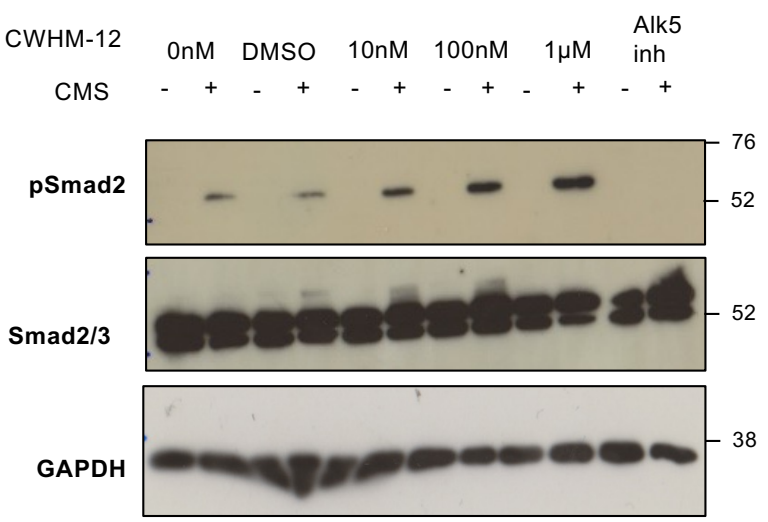
C)
CWHM-12
0nM
DMSO
10nM
100nM
1μM
Alk5 inh
CMS
- + - + - + - + - + - +
pSmad2
Smad2/3
GAPDH
76
52
52
38

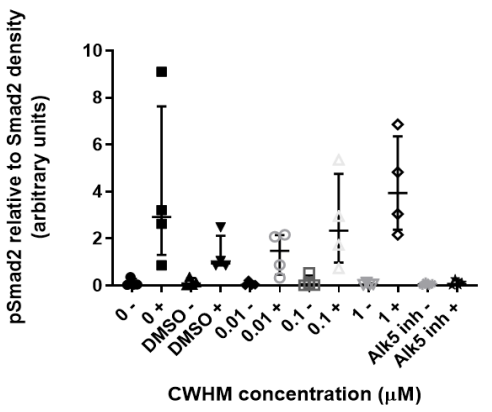
D)
pSmad2 relative to Smad2 density (arbitrary units)
0 2 4 6 8 10
0 - 0 + DMSO - DMSO + 0.01 - 0.01 + 0.1 - 0.1 + 1 - 1 + Alk5 inh - Alk5 inh +
CWHM concentration (μM)

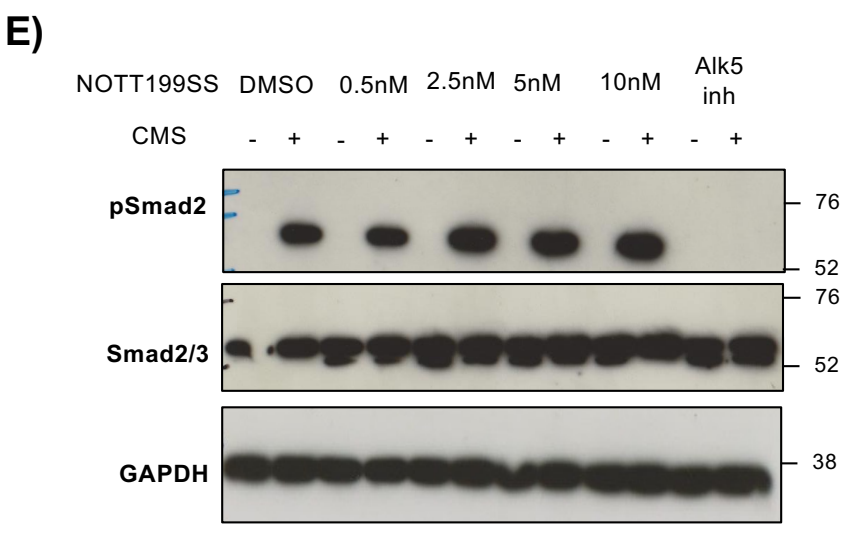
E)
NOTT199SS
DMSO
0.5nM
2.5nM
5nM
10nM
Alk5 inh
CMS
- + - + - + - + - + - +
pSmad2
Smad2/3
GAPDH
76
52
76
52
38

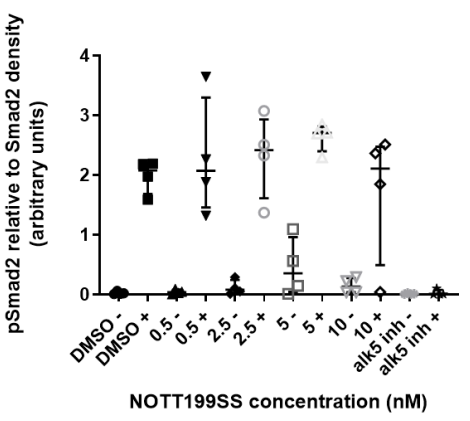
F)
pSmad2 relative to Smad2 density (arbitrary units)
0 1 2 3 4
DMSO - DMSO + 0.5 - 0.5 + 2.5 - 2.5 + 5 - 5 + 10 - 10 + alk5 inh - alk5 inh +
NOTT199SS concentration (nM)

Fig. S4. Cyclical stretch-induced TGFβ activation occurs independently of ROCK, and αv and β1 integrins in fibroblasts.

A) Representative pSmad2 western blot of human lung fibroblasts treated with the ROCK inhibitor Y27632 then subject to 48 hours of cyclical mechanical stretch (CMS) (15% elongation, 0.3Hz, 48 hours).

B) Relative pSmad2 to Smad2 densitometry from western blots of human lung fibroblasts treated with Y27632 then subject to cyclical stretch. Median ± interquartile range, n=4, two-tailed Mann Whitney test.

C) Representative pSmad2 western blot of human lung fibroblasts treated with an αv integrin inhibitor (CWHM-12) then subject to 48 hours of cyclical stretch (15% elongation, 0.3Hz, 48 hours).

D) Relative pSmad2 to Smad2 densitometry of human lung fibroblasts treated with CWHM-12 then subject to cyclical stretch. Median ± interquartile range, n=4, two-tailed Mann Whitney test.

E) Representative pSmad2 western blot of human lung fibroblasts treated with a β1 integrin inhibitor (NOTT199SS) then subject to 48 hours of cyclical stretch (15% elongation, 0.3Hz, 48 hours).

F) pSmad2 relative to Smad2 densitometry of human lung fibroblasts treated with NOTT199SS then subject to cyclical stretch. Median ± interquartile range, n=4, two-tailed Mann Whitney Test.

- + = stretched; - = unstretched; CMS= cyclical mechanical stretch; Y27632 = ROCK inhibitor; CWHM-12 = pan αv integrin inhibitor; NOTT199SS = β1 integrin inhibitor; DMSO = dimethyl sulfoxide; Alk5 inh = 50μM Alk5 inhibitor (SB525334)

Development • Supplementary information

Table S1. Resources and reagents used for this work

REAGENT or RESOURCE	SOURCE	IDENTIFIER
Antibodies		
Rabbit anti-phospho-Smad2 (pSmad2)	Cell Signaling Technology	Cat# 3808L
Rabbit anti-Smad2/3	Cell Signaling Technology	Cat# 3102
Rabbit anti-α-smooth muscle actin (αSMA)	Abcam	Cat# ab5694
Rabbit anti-GAPDH	Abcam	Cat# ab181603
Rabbit anti-TGFβ1	Abcam	Cat# ab92486
Rabbit anti-elastin	Atlas	Cat # HPA056941
Mouse anti-TGFβ2	Abcam	Cat# ab36495
Rabbit anti $G_{\alpha 11}$	Abcam	Cat# ab153951
Goat anti-$G_{\alpha q}$	Abcam	Cat# ab128060
HRP-conjugated goat-anti-rabbit	Agilent	Cat# P044801-2
HRP-conjugated rabbit-anti-goat	Agilent	Cat# P016002-2
HRP-conjugated rabbit anti-mouse	Agilent	Cat# P0260022-2
Rabbit anti-CD31	Abcam	Cat# ab182981
Rabbit anti-ki67	Abcam	Cat# ab15580
Rabbit anti-pro-surfactant protein C	Sigma	Cat# Ab3786
Rabbit anti-TGFβ2	Proteintech	Cat# 19999-1-AP
Biotinylated goat anti-rabbit IgG	Vector	Cat# BA1000
Chemicals, Peptides, and Recombinant Proteins		
Protein lysis buffer	Cell Signaling Technology	Cat# 9803
Phos-stop phosphatase inhibitors	Sigma	Cat# 04906837001
Complete mini protease inhibitors	Sigma	Cat# 04693124001
PMSF	Sigma	Cat# P7626
SB-525334 (ALK5 inhibitor)	Sigma	Cat# S8822

Development • Supplementary information

Y27632 (ROCK inhibitor)	Sigma	Cat# Y0503
CWHM-12 (αv integrin inhibitor)	A gift from Dr David Griggs, University of St Louis. Now commercially available from various suppliers	https://www.medchemexpress.com/CWHM-12.html https://medkoo.com/products/11038 https://www.caymanchem.com/product/19480/cwhm12
NOTT199SS	School of Chemistry at the University of Nottingham	n/a
GM6001 (MMP inhibitor)	Sigma	Cat# CC1010
DharmaFECT 1 transfection reagent	Dharmacon	Cat# T-2001-01
10% formalin	VWR	Cat# 11699404
Mayers haematoxylin	Sigma	Cat# S1275
Eosin	VWR	Cat# 101411-524
Hydrogen peroxide	VWR	Cat# 23619.264
SIGMAFAST(TM) 3,3'-Diaminobenzidine tablets	Sigma	Cat# D4418
AEBSF (serine protease inhibitor	Sigma	Cat# SBR00015
Western Restore Stripping Buffer	Thermo-Fisher	Cat# 21059
Ferric chloride (Iron(III) chloride)	Sigma	Cat# 157740
Iodine	Sigma	Cat# 326143
Potassium iodide	Sigma	Cat# 03124
Picric acid (in aqueous solution)	VWR	Cat# 84512.260
Acid fuschin	Sigma	Cat# F8129

Direct red 80	Sigma	Cat# 365548
Sodium thiosulphate	Scientific Laboratory Supplies	Cat# 72049
Haematoxylin	Sigma	Cat# H3136
Experimental Models: Cell Lines		
Human lung fibroblasts – primary cultures	Isolated and cultured in house (see methods for details)	n/a
Murine embryonic fibroblasts – wild-type	(Gu et al. 2002; Zywietz et al. 2001)	n/a
Murine embryonic fibroblasts – $Gnaq^{-/-}Gna11^{-/-}$	(Gu et al. 2002; Zywietz et al. 2001)	n/a
Murine embryonic fibroblasts – $Gna12^{-/-}$;$Gna13^{-/-}$	(Gu et al. 2002; Zywietz et al. 2001)	n/a
Experimental Models: Organisms/Strains		
Pdgfrb-$Cre^{+/-}$ mice	Generation described in (Foo et al. 2006)	n/a
Pdgfrb-Cre/$ERT2^{+/-+}$ mice	Jackson Laboratories	Cat # 029684
$Gnaq^{fl/fl}$;$Gna11^{-/-}$ mice	Generation described in (Offermanns et al. 1998; Wettschureck et al. 2001). Sperm stored in lab of origin.	n/a
Oligonucleotides		

Development • Supplementary information

Genotyping primers: Cre recombinase 5'- GCG GTC TGG CAG TAA AAA CTA TC – 3'; 5' - GTG AAA CAG CAT TGC TGT CAC TT – 3'	Eurofins (custom order)	n/a
Genotyping primers: internal positive control 5' - CTA GGC CAC AGA ATT GAA AGA TCT – 3' 5' - GTA GGT GGA AAT TCT AGC ATC C – 3'	Eurofins (custom order)	n/a
Genotyping primers: Gna11 wild type 5' – AGC ATG CTG TAA GAC CGT AG - 3' 5' – GCC CCT TGT ACA GAT GGC AG – 3'	Eurofins (custom order)	n/a
Genotyping primers: Gna11 knockout 5' - CAG GGG TAG GTG ATG ATT GTG – 3' 5' – GAC TAG TGA GAC GTG CTA CTT CC - 3'	Eurofins (custom order)	n/a
Genotyping primers: Gnaq 5' – GCA TGC GTG TCC TTT ATG TGA G 3' 5' – AGC TTA GTC TGG TGA CAG AAG – 3'	Eurofins (custom order)	n/a
Genotypring primers: Cre/ERT2 5'- GAA CTG TCA CCG GGA - 3' 5' - AGG CAA ATT TTG GTG TAC GG – 3'	Eurofins (custom order)	n/a
Human GNAQ siRNA (ON-TARGET-plus SMARTpool)	Dharmacon	Cat# L-008562-00-0005
Human GNA11 siRNA (ON-TARGET-plus SMARTpool)	Dharmacon	Cat# L-010860-00-0005
Non-targeting siRNA pool (ON-TARGET-plus SMARTpool)	Dharmacon	Cat# D-001810-10-05
Mouse Hprt primer forward: 5' – TGA AAG ACT TGC TCG AGA TGT CA - 3'	Eurofins (custom order)	n/a
Mouse Hprt primer reverse: 5' – CCA GCA GGT CAG CAA AGA ACT 3'	Eurofins (custom order)	n/a

Development • Supplementary information

Mouse Acta2 primer forward: 5’ - GGG ATC CTG ACG CTG AAG TA – 3’	Eurofins (custom order)	n/a
Mouse Acta2 primer reverse: 5’ – GAC AGC ACA GCC TGA ATA GC – 3’	Eurofins (custom order)	n/a
Mouse Eln primer forward: 5' GAT GGT GCA CAC CTT TGT TG 3'	Eurofins (custom order)	n/a
Mouse Eln primer reverse: 5' CAG TGT GAG CCA TCT CA 3'	Eurofins (custom order)	n/a
Mouse Col1a1 primer forward: 5' AGC TTT GTG CAC CTC CGG CT 3'	Eurofins (custom order)	n/a
Mouse Col1a1 primer reverse: 5' ACA CAG CCG TGC CAT TGT GG 3'	Eurofins (custom order)	n/a
Mouse Col3a1 primer forward: 5' TTT GCA GCC TGG GCT CAT TT 3'	Eurofins (custom order)	n/a
Mouse Col3a1 primer reverse: 5' AGG TAC CGA TTT GAA CAG ACT 3’	Eurofins (custom order)	n/a
Mouse *Pdgfa* primer forward: 5’ GAG ATA CCC CGG GAG TTG A 3’	Eurofins (custom order)	n/a
Mouse *Pdgfa* primer reverse: 5’ TCT TGC AAA CTG CAG GAA TG 3’	Eurofins (custom order)	n/a
Mouse *Pdgfb* primer forward: 5’ TGA AAT GCT GAG CGA CCA C 3’	Eurofins (custom order)	n/a
Mouse *Pdgfb* primer reverse: 5’ AGC TTT CCA ACT CGA CTC C 3’	Eurofins (custom order)	n/a
Mouse *Pdgfc* primer forward: 5’ AGG TTG TCT CCT GGT CAA GC 3’	Eurofins (custom order)	n/a
Mouse *Pdgfc* primer reverse: 5’ CCT GCG TTT CCT CTA CAC AC 3’	Eurofins (custom order)	n/a
Mouse *Pdgfd* primer forward: 5’CCA AGG AAC CTG CTT CTG AC 3’	Eurofins (custom order)	n/a

Development • Supplementary information

Mouse *Pdgfd* primer reverse: 5’ CTT GGA GGG ATC TCC TTG TG 3’	Eurofins (custom order)	n/a
Mouse *Pdgfra* primer forward: 5’ CAA ACC CTG AGA CCA CAA TG 3’	Eurofins (custom order)	n/a
Mouse *Pdgfra* primer reverse: 5’ TCC CCC AAC AGT AAC CCA AG 3’	Eurofins (custom order)	n/a
Mouse *Pdgfrb* primer forward: TGC CTC AGC CAA ATG TCA CC 3’	Eurofins (custom order)	n/a
Mouse *Pdgfrb* primer reverse: 5’ TGC TCA CCA CCT CGT ATT CC 3’	Eurofins (custom order)	n/a
Human GNAQ primer forward: 5’ – GGACAGGAGAGGGTGGCAAG – 3’	Eurofins (custom order)	n/a
Human GNAQ primer reverse: 5’ – TGGGATCTTGAGTGTGTCCA – 3’	Eurofins (custom order)	n/a
Human GNA11 primer forward: 5’ – CCACTGCTTTGAGAACGTGA – 3’	Eurofins (custom order)	n/a
Human GNA11 primer reverse: 5’ GCAGGTCCTTCTTGTTGAGG – 3’	Eurofins (custom order)	n/a
Human B2M primer forward: 5’-AATCCAAATGCGGCATCT-3’	Eurofins (custom order)	n/a
Human B2M primer reverse: 5’-GAGTATGCCTGCCGTGTG-3’	Eurofins (custom order)	n/a
Software and Algorithms		
Image J	NIH	https://imagej.nih.gov/ij/
NIH Elements v3.2	Nikon	https://www.microscope.healthcare.nikon.com/products/software/nis-elements/viewer

MicroManager 1.4	Vale lab, UCSF	https://micro-manager.org/
CaseViewer 2.3	3D Histech	https://www.3dhistech.com/
Prism	Graphpad	https://www.graphpad.com/scientific-software/prism/
Other		
Goat serum	Sigma	Cat# G9023
Avidin-Biotin complex	Vector	Cat# SP2001
DPX mountant	Sigma	Cat# 06522
Phosphate buffered saline	Sigma	Cat# P4417
Nikon 90i microscope	Nikon	n/a
Axioplan microscope	Zeiss	n/a
Dulbecco's modified eagles medium	Sigma	D5671
Foetal Calf Serum	Harlan UK Ltd	S-0001AE
L-glutamine	Sigma	G7513
Penicillin/ streptomycin	Sigma	P4458
Amphotericin B	Sigma	Cat# A2942
Collagen I-coated Bioflex® 6 well culture plates	Dunn Labortechnik	Cat# 3001-C
Flexcell® cell stretching system	Flexcell International Corporation	Cat# FX-5000T
BCA Assay kit	ThermoFisher	Cat# PN23227
Nucleospin RNA isolation kit	Machery-Nagel	Cat# 740955.250
Superscript IV Reverse Transcriptase	ThermoFisher	Cat# 18090050
KAPA SYBR FastTaq	Sigma	Cat# KK4618
PerfeCTa® SYBR Green Fastmix	VWR	Cat# 733-1382
MXPro3000 qPCR machine	Stratagene	

Development • Supplementary information

Heparin sodium 5000 units/ml	Wockhardt	Cat# FP1083
Polyvinylidene fluoride membrane	BioRad	Cat# 1620177
Hyperfilm for western blots	GE Healthcare	Cat# 28-9068-35
ECL reagent	GE Healthcare	Cat# RPN2134
Clarity ECL	BioRad	Cat# **1705061**
Tamoxifen-containing chow (400mg/kg tamoxifen citrate)	Envigo	Cat# TD.55125.1

Development • Supplementary information